J. Fluid Mech. (1995), vol. 283, pp. 365–407

Experimental investigation of subharmonic resonance in an axisymmetric jet

By C. O. PASCHEREIT[1]†, I. WYGNANSKI[2], AND H. E. FIEDLER[1]

[1]Hermann-Föttinger-Institut, Technische Universität Berlin, 10623 Berlin, Germany

[2]Aerospace & Mechanical Engineering Department, University of Arizona, Tucson, USA and the Department of Fluid Dynamics, Tel-Aviv University, Tel-Aviv, Israel

(Received 29 July 1994 and in revised form 19 September 1994)

A resonant subharmonic interaction between two axisymmetric travelling waves was induced in the shear layer of an axisymmetric jet by controlled sinusoidal perturbations with two frequencies separated by one octave. Wherever the two excited waves are non-dispersive and the fundamental is close to its linear neutral point the two waves may interact in a manner that enhances the amplification rate of the subharmonic wave train. The amplified subharmonic will exceed the fundamental's level to become the dominant instability component. The initial phase difference between the subharmonic and the fundamental plays an important role in the amplification of the subharmonic. For specific phase angles between the two excited waves a suppression of the subharmonic may be observed. The influence of other initial parameters such as amplitude ratio, overall forcing level, excitation frequency and flow conditions at the nozzle (i.e. the initial turbulence level and the initial momentum thickness) was also investigated. An increase in the combined forcing level reduces the effect of the initial phase difference on the amplification of the subharmonic. Stronger excitation moves the location at which the two waves are locked in space further upstream while the effect of the initial phase difference decreases. The energy transfer to the subharmonic wave has been analysed by estimating the production terms. The results clearly indicate that most of the energy for the resonant growth of the subharmonic comes directly from the mean flow. The fundamental wave acts as a catalyst, as long as the resonance conditions are satisfied, enhancing the rate of energy transfer from the mean flow to the subharmonic.

1. Introduction

The instability of jets is a phenomenon which is not only relevant to the fundamental understanding of turbulence, but it is also a technologically important flow in which mixing and noise production occurs. The response of a jet to artificial excitation is of practical interest to turbulence control. Major contributions toward understanding and prediction of noise production were made by Michalke (e.g. 1971, 1972, 1977, 1984, 1992).

The development of the thin axisymmetric shear layer of a jet near the nozzle is dominated by a linear instability mechanism as first discussed by Kelvin and

† Present address: ABB Corporate Research Center, Aerodynamics Department, 5405 Baden, Switzerland.

Helmholtz for low Reynolds number flows. The travelling instability waves grow in the direction of streaming until they reach a finite amplitude and then they roll up into discrete vortices as predicted by Michalke (1965) and experimentally verified by Freymuth (1966). The thin axisymmetric shear layer close to the nozzle is unstable to a large number of modes (Plaschko 1979; Cohen & Wygnanski 1987*a*) while the fully developed jet at some distance from the end of the potential core is unstable only to the first helical mode, $m = 1$ (Batchelor & Gill 1962). Michalke (1971), Fuchs (1972) and Mattingly & Chang (1974) recognized the potential importance of the helical mode which should have been amplified in an axisymmetric jet at rates that are comparable to the amplification rates of the plane ($m = 0$) mode of instability. A systematic study by Strange (1981) showed that the growth rates of the modes $m = 0$ and $m = 1$ are indeed comparable.

Active control of the flow can be achieved by external excitation. Not only is the spreading rate of the jet influenced in this way, but also the mixing on the molecular scale and therefore the rate of chemical reaction is enhanced (Roberts 1984). The range of distances at which mixing is increased depends on the frequency and the amplitude of the excitation as well as on other parameters of the primary motion. The first comprehensive study of the response of an axisymmetric jet to a controlled axisymmetric ($m = 0$) excitation was done by Crow & Champagne (1971). They observed that an amplified instability wave also increases the rate of spread of the flow in the direction of streaming. Increasing the forcing amplitude beyond the level required to achieve saturation at some location downstream, while keeping all other flow parameters constant, does not enhance the growth of the fundamental instability wave beyond its nominal saturation level and therefore has no additional effect on the mixing process (see also Oster & Wygnanski 1982; Fiedler & Mensing 1985; Weisbrot & Wygnanski 1988). The degree of control is therefore limited as long as only one frequency is excited.

Further enhancement of mixing can be achieved by a concomitant excitation of a second instability wave, e.g. its subharmonic. When the fundamental becomes neutrally stable, its subharmonic, which amplifies linearly at a very high rate (figure 1*a*), enhances the mixing. Second-order interactions between a high-amplitude fundamental wave and a low-amplitude subharmonic may lead to resonance (Kelly 1967), and result in an enhanced growth of the subharmonic above the predictions of the linear stability theory. The augmentation of the subharmonic wave contributes to an additional enhancement of the mixing. Thus, combined-mode forcing is not only relevant to the fundamental understanding of turbulence, but also to the technologically important problem of mixing and turbulence control.

Michalke (1984) derived the conditions under which two axisymmetric disturbances ($m = 0$) can resonate in an axisymmetric shear layer. Cohen & Wygnanski (1987*b*) extended the analysis to allow azimuthal disturbances to interact. They found that for subharmonic resonance both waves must propagate with identical phase speeds and thus the high-amplitude fundamental must be close to its neutral point according to linear stability theory (figure 1*a*, *b*). Cohen & Wygnanski verified this condition experimentally by exciting a jet at a single frequency but at different azimuthal modes. Wherever the phase velocities of the excited fundamental and the naturally growing subharmonic were identical a band of frequencies centred around the subharmonic frequency was enhanced. Conversely, at locations at which the two waves were dispersive no significant response at the subharmonic frequency was found. Cohen & Wygnanski did not investigate the energy transfer to the subharmonic in detail. Monkewitz (1988) suggested that for the particular case of subharmonic resonance

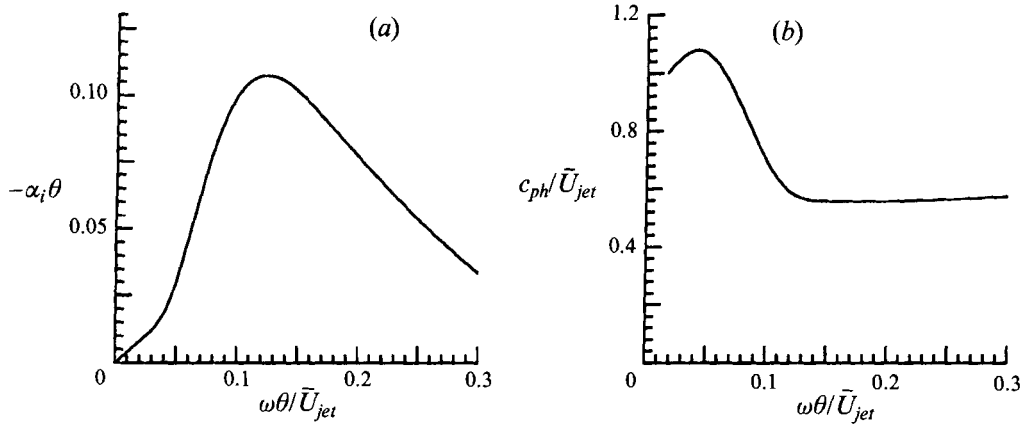

FIGURE 1. Calculated growth rates (*a*) and phase speed (*b*) of the axisymmetric component. Reprinted from Cohen & Wygnanski (1987*b*)

the energy transfer is parametric and thus the amplitude of the fundamental remains unchanged and the energy for the subharmonic is supplied by the mean flow which is assumed to remain constant by virtue of the parallel flow assumption.

In order to investigate laminar–turbulent transition, Miksad (1972, 1973) excited a shear layer with two frequencies of comparable growth rates. The two waves interacted nonlinearly, generating harmonics and subharmonics of the forcing frequencies. Ronneberger & Ackermann (1979) measured the sound radiation of a turbulent jet excited at two frequencies. However, they did not investigate the influence of the initial phase alignment on the amplification of the instability waves. Theoretical derivations of temporal instability in a shear layer (Patnaik, Sherman & Corcos 1976) and spatial instability (Monkewitz 1988) in a plane mixing layer showed that the wave–wave interaction is highly dependent on such phase alignment. The influence of the initial phase difference was observed experimentally by Arbey & Ffowcs Williams (1984). They found that the subharmonic is suppressed when the initial phase difference is 45°. A dependence of the amplification of the subharmonic on the initial phase difference was also established by Bradly & Ng (1989), who observed a suppression of the subharmonic for an initial phase difference of 45°. Raman & Rice (1989) found the suppression of the subharmonic for certain phase angles to be dependent on the Strouhal number of the forced waves. Hajj, Miksad & Powers (1993) investigated the influence of four initial phase differences on the subharmonic in a two-stream mixing layer forced at relatively low levels. They presented the evolution of phase-locked data taken at one cross-stream location and observed a suppression of the resonant subharmonic when the initial phase difference was 104°.

However, those studies examined only a few limited conditions in which mostly high forcing levels were used. In the experiment of Bradly & Ng the velocity perturbation on the centreline of the jet at the nozzle exit was 1.4%; it was 2% in the experiment of Arbey & Ffowcs Williams. Raman & Rice forced the fundamental at levels varying between 3% and 7%. Since there are more parameters which influence the growth of the subharmonic and more ways in which resonance may be generated, one has to be careful in identifying the correct physical mechanism involved.

The present paper describes a detailed investigation of the interaction between subharmonic and fundamental waves close to the nozzle of the jet. A large quantity of data was taken in both radial and streamwise directions to describe the development

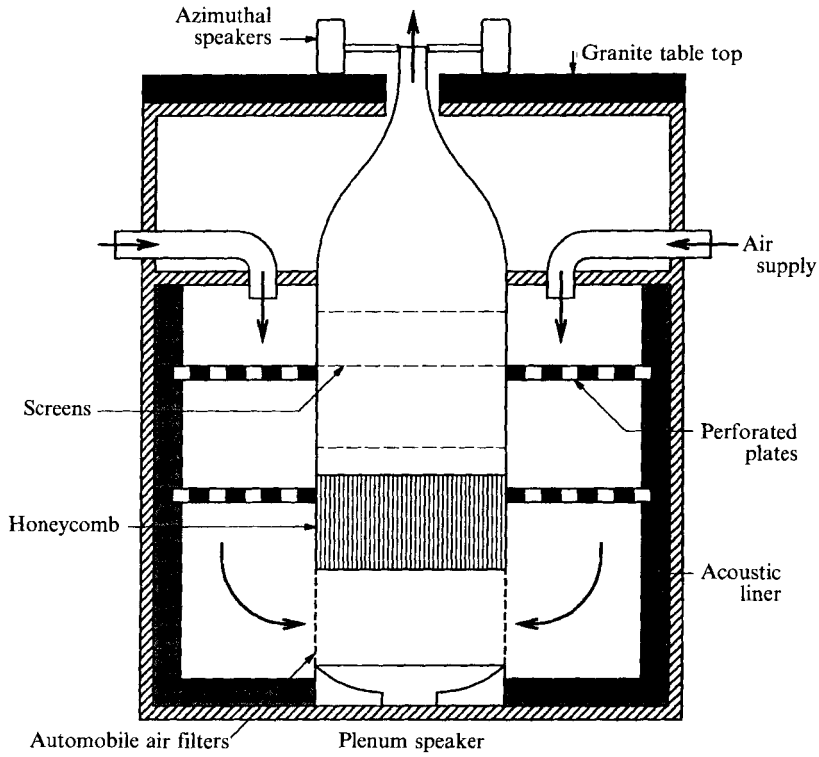

FIGURE 2. The air jet facility.

of the subharmonic wave. The forcing amplitudes were kept low: the maximum amplitude of the phase-locked fundamental in the centre of the shear layer was 3.2% at $x/D = 0.25$, while the amplitude on the jet centreline was less than 0.02%. The influence of the initial phase difference has been studied for a variety of forcing levels, and frequency pairs. Additional experiments were made when the turbulence in the developing shear layer was increased by a trip ring installed inside the nozzle.

In his analysis Kelly implicitly fixed and decoupled the fundamental wave from the rest of the flow. This prompted us to investigate the energy transfer among the instability waves themselves and between the waves and the mean flow.

2. Description of the experiments

2.1. *Jet facility*

A cross-section of the plenum chamber and the jet nozzle is shown in figure 2. The plenum chamber contains perforated plates, two air filters, a honeycomb straightener, and three screens to reduce the turbulence level of the flow upstream of the contraction. The contraction ratio of the nozzle is 36:1, its exit diameter being $D = 50.8$ mm. The nozzle contour is described by two tangent arcs and its exit is extended by a parallel section one diameter in length. The air flow of the jet was supplied by a blower with a Toshiba VF Pack P1 speed controller which provided a stable air source. The exit velocity in the present experiment is $\overline{U}_{jet} = 8$ m/s, corresponding to a Reynolds number, based on the nozzle diameter, of $Re_D = 28\,000$. At 8 m/s, the free-stream turbulence level is 0.097%. The jet emerges with a 'top-hat' velocity profile

surrounded by a thin shear layer. Both jet and measuring apparatus are enclosed in a large cage of 1/6 mm mesh screen to minimize the effect of room draughts.

2.2. *Experimental methods*

The facility was instrumented with a ring of eight normal hot wires equally spaced around the circumference at 45° apart and capable of measuring the streamwise component of velocity. The probe locations are expressed in cylindrical coordinates (r, φ, x) where r is the radial distance to the centreline, φ the polar angle, and x is the streamwise distance from the nozzle. The eight probe holders were mounted on separate micrometer screws and could be adjusted independently in both radial and axial directions. The traversing mechanism was then capable of moving all sensors simultaneously for equal distances in the radial direction. The radial motion was accomplished by a computer controlled stepper motor. The ring assembly could be translated in the axial direction along three posts aligned parallel to the jet centreline. The streamwise position of the probes was determined by an optical cathetometer.

The hot wires were made of 5 μm tungsten wire with an aspect ratio of 300. The locally built anemometers were operated in the constant temperature mode at an overheat ratio of 1.8. All signals were low pass filtered at 10 kHz, amplified and converted in an analog-to-digital converter. A Masscomp 5500 PEP computer was used for data acquisition and primary data evaluation. It has 16 channels of analog-to-digital converters with a maximum aggregate sampling rate of 1 Mhz and 8 channels of digital-to-analog converters with a maximum aggregate rate of 200 kHz. The system was able to generate simultaneously the forcing signal and a subharmonic reference signal to the digital-to-analog channels while collecting and processing the data.

Controlled axisymmetric excitation (mode $m = 0$) of the jet was accomplished by a loudspeaker used as a compression driver and located at the bottom of the plenum chamber. The excitation signals were generated on the laboratory computer by superimposing two sine waves separated by one octave in frequency and variable relative phase. Certain axisymmetric disturbances are amplified in the plenum chamber at Helmholtz resonance condition. Since it was the purpose of this experiment to isolate the subharmonic resonance in the shear layer it was necessary to avoid plenum resonances which could mask the resonance effects investigated. Therefore the response of the apparatus to Helmholtz resonances was determined *a priori* and the critical frequencies were avoided in the experiment. In any case the upstream boundary conditions at the nozzle exit were determined.

2.3. *Processing of the data*

The hot wires were calibrated close to the exit plane of the jet against the velocity determined by the static pressure in the plenum chamber. A MKS Baratron pressure transducer was used for this purpose. A third-order polynomial was fitted to seven velocities ranging from 50 mm/s to 900 mm/s measured by each anemometer. The calibration procedure was automated and controlled by the laboratory computer. The conditioned signals from the eight hot-wire probes were passed through the analog-to-digital converters and converted to velocities using the calibration polynomials on a vector accelerator. Each buffer of data was then phase-averaged with respect to the reference signal and stored on disk.

In the presence of coherent motion, any variable, like the streamwise velocity, may be decomposed into three parts (Hussain & Reynolds 1970): a steady mean flow, a

coherent component and a random fluctuation, viz.

$$u_i(x_j, t) = \overline{U}_i(x_j) + \tilde{u}_i(x_j, \tau) + u_i'(x_j, t), \tag{2.1}$$

where the phase-locked average $\langle u_i \rangle = \overline{U}_i + \tilde{u}_i$ and the random component $\overline{u_i'^2} = \overline{(u_i - \langle u_i \rangle)^2}$.

The coherent data were then decomposed into complex Fourier coefficients, $F_{mn}(r)$, defined by

$$F_{mn} \equiv \frac{1}{2\pi T} \int_0^{2\pi} \int_0^T \langle u(r_i, \varphi, \tau) \rangle e^{i[m\varphi - \omega\tau]} \, d\varphi d\tau, \tag{2.2}$$

from which the magnitude and the phase ϕ of the measured signal can be obtained. Thus, $|F_{01}(r_i)|$ is the magnitude at the radial position $r = r_i$ of the mode $m = 0$ of the flow of the recorded u signal. Since only axisymmetric modes ($m = 0$) were considered in this study, the magnitude is $|\tilde{u}|$.

The traversing mechanism only allowed the use and calibration of single-wire probes *in situ*, therefore it was only possible to measure the streamwise velocity components. Since in the axisymmetrically forced case $\overline{W} \approx 0$ and also $\tilde{w} \approx 0$ each component of the decomposed velocity independently satisfies the continuity equation

$$\frac{\partial \overline{U}}{\partial x} + \frac{1}{r} \frac{\partial (r\overline{V})}{\partial r} = \frac{\partial \tilde{u}}{\partial x} + \frac{1}{r} \frac{\partial (r\tilde{v})}{\partial r} = 0, \tag{2.3}$$

from which the radial components could then be calculated.

2.4. *Summary of the experiments*

The main objective of this work was to determine the significance of the inflow parameters. Prompted by the experiments of Arbey & Ffowcs Williams (1984) and theoretical work by Monkewitz (1982, 1988), who had suggested that the initial phase difference between a fundamental wave and its subharmonic is important to the growth of the subharmonic, we set forth to verify this suggestion. All theoretical models assume that small disturbances are superimposed on a parallel mean flow. In a diverging mixing layer the phase speed is, however, not constant across the shear layer, i.e. the phase advances more rapidly on the high-speed side of the mixing layer than on the low-speed side. This might violate the resonance condition, which requires that the two interacting waves will be non-dispersive, and might influence the development of the subharmonic. It was therefore important to investigate the influence of the spreading rate of the mixing layer, the initial amplitude ratio of the forced waves and the overall forcing level on the resonant interaction.

A compilation of the numerous experiments carried out with different frequencies and amplitude ratios $\gamma = A_{sub}/A_{fun}$, forcing levels and other information (e.g. the conditions at the nozzle) is presented in table 1. All experiments were done with an exit velocity of $\overline{U}_{jet} = 8$ m/s. Because the initial phase difference is an important parameter which influences the development of the subharmonic wave, all bimodal forcing cases were carried out at least two or more different initial phase differences. Note that the term 'high forcing level' is used when the maximum phase-locked fluctuation of the fundamental wave reached 3.2% of the mean velocity in the centre of the shear layer at $x/D = 0.25$ corresponding approximately to 0.02% in the centre of the jet column and is therefore near the limit of the resolution of the measurement. We refer to it as 'high-amplitude forcing', being twice the amplitude of most other cases.

No.	Case	St_D	$\left.\frac{\lvert\tilde{u}\rvert_{max}}{\overline{U}_{jet}}\right\rvert_{x/D=0.25}$	$\left.\frac{\int_{r=0}^{r_{0.1}} \lvert\tilde{u}_{sub}\rvert^2 + \lvert\tilde{u}_{fun}\rvert^2 r\,dr}{\overline{U}_{jet}^2 D^2}\right\rvert_{x/D=0.25}$
I	184 Hz, forcing level as in *III*	1.2	0.3%	1.1×10^{-7}
II	368 Hz, forcing level as in *III*	2.3	1.6%	2.1×10^{-6}
III	184 & 368 Hz, $\gamma = 1.6$	2.3	1.6%	2.1×10^{-6}
IV	184 & 368 Hz, $\gamma = 0.4$	2.3	1.6%	2.1×10^{-6}
V	184 & 368 Hz, $\gamma = 0.1$	2.3	1.6%	2.1×10^{-6}
VI	high forcing 184 & 368 Hz, $\gamma = 0.1$	2.3	3.2%	13.2×10^{-6}
VII	data along centreline 184 & 368 Hz, $\gamma = 0.1$	2.3	$\left.\frac{\lvert\tilde{u}\rvert}{\overline{U}_{jet}}\right\rvert_{x/D=0.2,r=0} = 0.5\%$	
VIII	data along centreline 62 & 124 Hz, $\gamma = 0.1$	0.8	$\left.\frac{\lvert\tilde{u}\rvert}{\overline{U}_{jet}}\right\rvert_{x/D=0.2,r=0} = 1.7\%$	
IX	data along centreline 31 & 62 Hz, $\gamma = 0.1$	0.4	$\left.\frac{\lvert\tilde{u}\rvert}{\overline{U}_{jet}}\right\rvert_{x/D=0.2,r=0} = 2.7\%$	
X	trip ring, low forcing 184 & 368 Hz, $\gamma = 1.6$	2.3	1.3%	2.0×10^{-6}
XI	trip ring 184 Hz, forcing level as in *XIII*	1.2	0.7%	5.7×10^{-7}
XII	trip ring 368 Hz, forcing level as in *XIII*	2.3	6.1%	7.4×10^{-6}
XIII	trip ring 184 & 368 Hz, $\gamma = 1.6$	2.3	6.5%	$46. \times 10^{-6}$
XIV	140 & 280 Hz, $\gamma = 1.6$	1.8	1.1%	2.1×10^{-6}
XV	150 & 300 Hz, $\gamma = 1.6$	1.9	1.1%	2.1×10^{-6}

TABLE 1. Compilation of the experiments.

3. Subharmonic resonance

3.1. *Resonance conditions for the axisymmetric jet*

Under the assumption of parallel flow Cohen & Wygnanski (1987*b*) examined the conditions for resonance interactions between two instability waves. Following Kelly (1967), they found that if $\boldsymbol{q}_{out}$ represents a secular, growing wave produced by the interaction between the waves $\boldsymbol{q}_1$ and $\boldsymbol{q}_2$, the eigenvalues associated with $\boldsymbol{q}_{out}$ must satisfy one of the following interaction conditions†

$$\alpha_{out} = \alpha_1 + \alpha_2;\ \omega_{out} = \omega_1 + \omega_2;\ m_{out} = m_1 + m_2, \tag{3.1}$$

$$\alpha_{out} = \alpha_1 - \alpha_2^*;\ \omega_{out} = \omega_1 - \omega_2;\ m_{out} = m_1 - m_2, \tag{3.2}$$

† These conditions are often referred to as resonance conditions in the literature (Kelly 1967; Cohen & Wygnanski 1987*b*). The word resonance is used only for convenience; it does not necessarily imply an increase in growth rate. It would indeed be more accurate to call them interaction conditions.

where α is the wavenumber. The interaction between two waves of the same frequency but opposite mode numbers may lead to a distortion of the mean flow (e.g. Long & Petersen 1992; Paschereit *et al.* 1992).

For axisymmetric disturbances the output mode number $m_{out} = m_{fun} - m_{sub} = 0$ is also axisymmetric and the resonance conditions reduce to

$$c_{ph,fun} = c_{ph,sub} \tag{3.3}$$

and

$$\alpha_{i,sub} = \alpha_{i,fun} + \alpha_{i,sub}\,, \tag{3.4}$$

where the subscripts *fun* and *sub* represent the fundamental and the subharmonic wave respectively and c_{ph} is the phase velocity of the wave defined by $c_{ph} = \omega/\alpha_r$. These conditions suggest that for a subharmonic to be in resonance with its fundamental, both waves must propagate with the same phase speed *and* the fundamental must be close to its neutral point to satisfy equation (3.4). First experimental verification was obtained by forcing the jet with a single (fundamental) frequency of $f = 368$ Hz (case *II*). Downstream of $x/D > 0.56$, at $St_{\theta,fun} \approx 0.3$, the resonance conditions (3.3) and (3.4) were met (figure 1*a* and figure 1*b*); consequently for a narrow band of frequencies around the subharmonic frequency ($f = 184$ Hz) an increase of energy was observed (figure 3*a*). Conversely, forcing at a frequency of $f = 184$ Hz (case *I*) did not produce any significant wave at the corresponding subharmonic frequency of $f = 92$ Hz (figure 3*b*): For $St_{\theta,fun} = 0.15$ the resonance conditions are not satisfied and no resonant interaction could be expected.

3.2. *Radial profiles of the phase-averaged modulus*

Radial profiles of the modulus of the decomposed phase-averaged velocities normalized by the exit jet velocity, $|\tilde{u}|/\overline{U}_{jet}$, are plotted in figure 4 for two downstream positions $x/D = 0.3$ and $x/D = 0.8$. The radial distance was normalized by the local momentum thickness and the origin of the coordinate system was shifted to the centre of the shear layer by defining the radius of the jet column $R_{0.5}$ as the radial distance at which the local mean velocity is one-half of its value on the centreline $\overline{U}_{cl}$. Thus:

$$\eta = \frac{r - R_{0.5}}{\theta}\,, \tag{3.5}$$

where the momentum thickness is defined as

$$\theta = \int_{r=0}^{r_{0.1}} \frac{\overline{U}(r)}{\overline{U}_{cl}} \left(1 - \frac{\overline{U}(r)}{\overline{U}_{cl}}\right) \mathrm{d}r\,. \tag{3.6}$$

In this study the centreline velocity was equal the jet exit velocity $\overline{U}_{jet}$ since all measurements were done in the region of the potential core ($x/D < 3$). Following Long & Peterson (1992) the above integral was truncated at the radial position where $\overline{U}(r) = 0.1\overline{U}_{jet}$ because the hot-wire calibrations were inaccurate below this level. This truncation was used for all transverse integrations.

Let us consider now three specific cases of forcing: (*i*) forcing of the subharmonic $f_{sub} = 184$ Hz only (case *I*), (*ii*) forcing of the fundamental $f_{fun} = 368$ Hz only (case *II*) and (*iii*) both waves forced simultaneously with an initial amplitude ratio of $\gamma = A_{sub}/A_{fun} = 1.6$ and an initial phase difference of $\Delta\phi = 0°$.

At $x/D = 0.3$ the Strouhal numbers of the subharmonic and the fundamental based on the momentum thickness are $St_{\theta,sub} = 0.08$ and $St_{\theta,fun} = 0.16$ respectively.

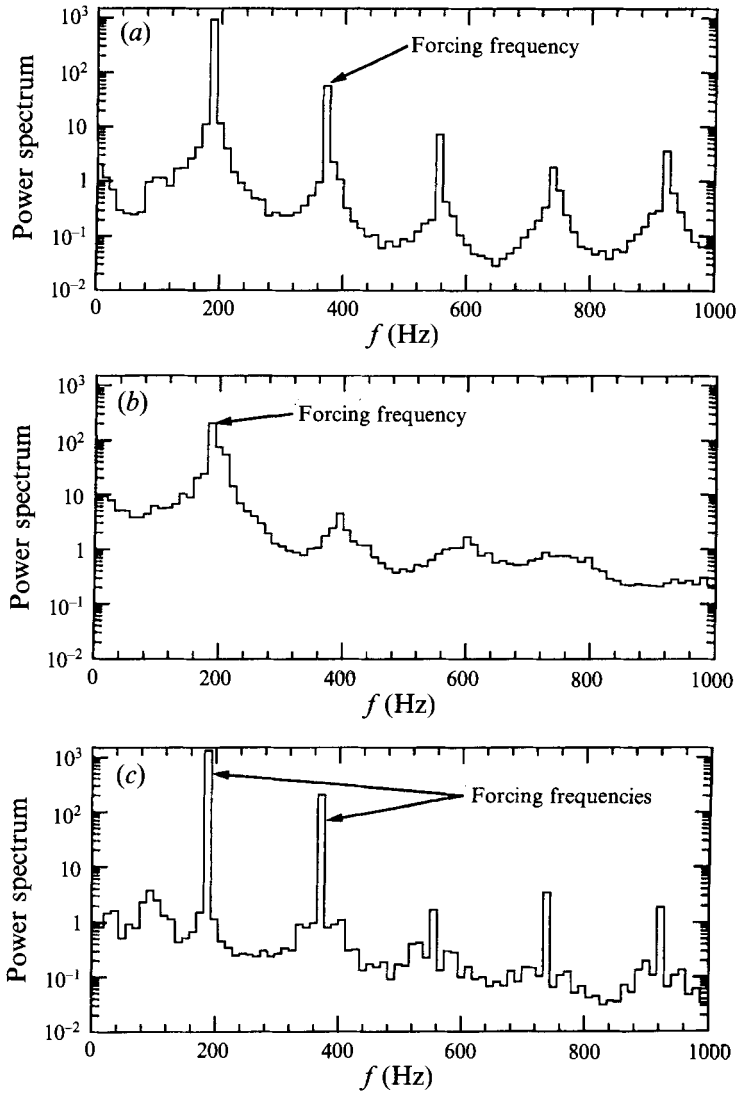

FIGURE 3. Power spectra at $x/D = 0.8$, $\overline{U}/\overline{U}_{jet} = 0.5$ for the jet forced with (*a*) 368 Hz (case *II*), (*b*) 184 Hz (case *I*) and (*c*) 184 and 368 Hz (case *III*).

There, both frequencies are amplified linearly (figure 4*a–c*). The growth rate of the fundamental, being higher than the growth rate of the subharmonic (figure 1), leads to the higher amplitude of the fundamental wave for all three forcing cases. The resonance conditions (3.3) and (3.4) are not satisfied and therefore the subharmonic amplitudes (figures 4*a* and 4*c*) are not affected by the presence or absence of the fundamental (generated at $f = 368$ Hz).

At $x/D \approx 0.53$ the Strouhal numbers of the subharmonic and the fundamental are $St_{\theta,sub} = 0.15$ and $St_{\theta,fun} = 0.3$ respectively and thus both resonance conditions are met. The radial amplitude distribution of the instability waves measured at $x/D = 0.8$ is shown in figure 4(*d–f*) (note also the different scale of the ordinate in figure 4*d–f* relative to 4*a–c*). The subharmonic amplitude was enhanced by a factor of 2.5 when the jet was forced simultaneously at both frequencies $f = 184$ and 368

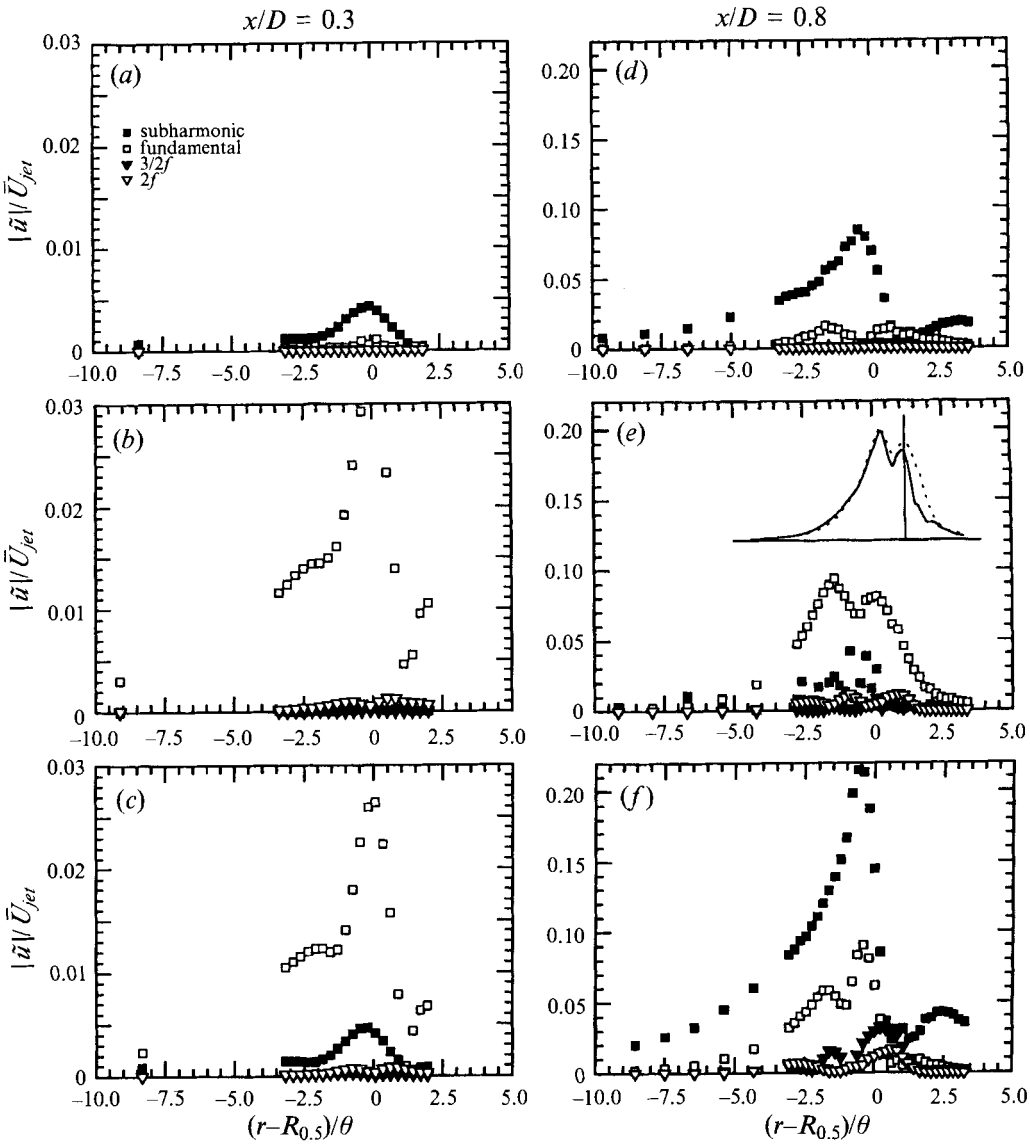

FIGURE 4. Radial profiles of the phase-averaged modulus of the different modes at two downstream locations. The jet was forced at 184 Hz (case *I*) (*a*, *d*), 368 Hz (case *II*) (*b*, *e*) and simultaneously at 184 Hz and 368 Hz (case *III*) (*c*, *f*). The insert in (*e*) compares the radial profiles of the fundamental forced alone (case *II*) (dotted line) and the fundamental generated by bimodal forcing (case *III*) (solid line) at identical *Strouhal numbers*.

Hz rather than at a single frequency $f = 184$ Hz of identical amplitude. Bimodal forcing enhanced the development of the $\frac{3}{2}f_{fun} = 552$ Hz mode also (figures 3 and 4*f*). This is consistent with the sum interaction condition (equation (3.1)), which leads to the amplification of the frequency $(f_{sub} + f_{fun}) = \frac{3}{2}f_{fun}$. Single-frequency forcing of the fundamental wave leads to the development of a subharmonic (figure 4*e*) of, however, small amplitude. Forcing at the fundamental frequency of $f = 368$ Hz only, results in an amplification of a broader band of frequencies around the subharmonic (see the plots of the power spectrum, figure 3*a*) whereas forcing at both frequencies

(f = 184 and 368 Hz) focusses on the amplification making the spectral peak of the subharmonic (see figure 3*c*) much clearer defined. Bimodal forcing increases the momentum thickness $\theta_{0.1}$ more strongly than forcing at the fundamental alone and in turn the disturbance Strouhal number St_θ increases at the same x/D. Because of the different St_θ values the radial amplitude distributions of the jet forced at the fundamental frequency alone (figure 4*e*) and at both frequencies (fundamental and subharmonic) look different (figure 4*f*) because they correspond to different locations on the stability diagram and are therefore represented by different eigenfunctions. When the two modes are compared at the same Strouhal number the shapes of the amplitude distributions are similar (see the insert in figure 4*e* showing these shapes). The dotted line corresponds to the fundamental at conditions described in figure 4(*e*) and the solid line represents the fundamental generated by bimodal forcing at conditions corresponding to figure 4(*f*) but at a streamwise location corresponding to $x/D = 0.75$ where St_θ for both forcing stations is the same.

3.3. *Streamwise evolution of the instability modes*

The streamwise evolution of the instability modes helps us to understand the effects of the resonance. The following three criteria which are commonly used in the literature (Cohen & Wygnanski 1987*a*; Petersen 1978; Gaster, Kit & Wygnanski 1985) serve as measures of the energy (or amplitude) of a given wave at a given streamwise cross-section (figure 5):

$$\frac{|\tilde{u}|_{max}}{\overline{U}_{jet}}, \quad \frac{1}{\overline{U}_{jet}D^2}\int_{r=0}^{r_{0.1}} |\tilde{u}|\, r\, \mathrm{d}r, \quad \frac{1}{\overline{U}_{jet}^2 D^2}\int_{r=0}^{r_{0.1}} |\tilde{u}|^2\, r\, \mathrm{d}r\,. \tag{3.7a–c}$$

They display qualitatively the same trend but their maxima occur at different streamwise locations. The maximum amplitude of the subharmonic is at $x/D = 0.78$ (figure 5*a*) while the maximum for the integrated amplitudes occurs at $x/D \approx 0.9$ (figure 5*b*) and the maximum energy occurs somewhat earlier at $x/D = 0.84$ (figure 5*c*). The subharmonic ceases to amplify by the linear instability mechanism at $x/D = 0.84$, which is also evident from the shape of the radial amplitude distribution plotted in figure 5(*c*). Since the neutral point coincides with the maximum energy level attained, the energy criterion is preferred in displaying the evolution of the instability. The streamwise location of the maxima of the subharmonic obtained by the two other criteria given in equations (3.7*a*) and (3.7*b*) is thus either upstream or downstream of the linearly neutral amplification point, respectively. This is also evident from the shape of the radial amplitude distribution (figures 5*a* and 5*b*) which does not correspond to the shape of the neutrally stable amplitude distribution in these two instances. The reason for the maxima calculated by the three criteria occurring at different x-locations is due to the change in the radial shape of the amplitude distribution. Thus the description using maximum amplitude (equation (3.7*a*)) may be misleading because it does not take the spreading of the shear layer into account. The maximum amplitude may decrease even though the energy contained in the specific mode when integrated over the shear layer actually increases. Furthermore, since the shape of the radial amplitude profile changes with distance from the nozzle a second peak might develop (as shown in figure 4*e*) which exceeds the original peak used to characterize the amplitude in the centre of the shear layer. The fundamental wave is neutrally stable at $x/D = 0.53$. The corresponding 'neutral' amplitude distribution of the fundamental is displayed in figure 5(*c*).

All three 'measures' show a rapid increase of the subharmonic wave due to the res-

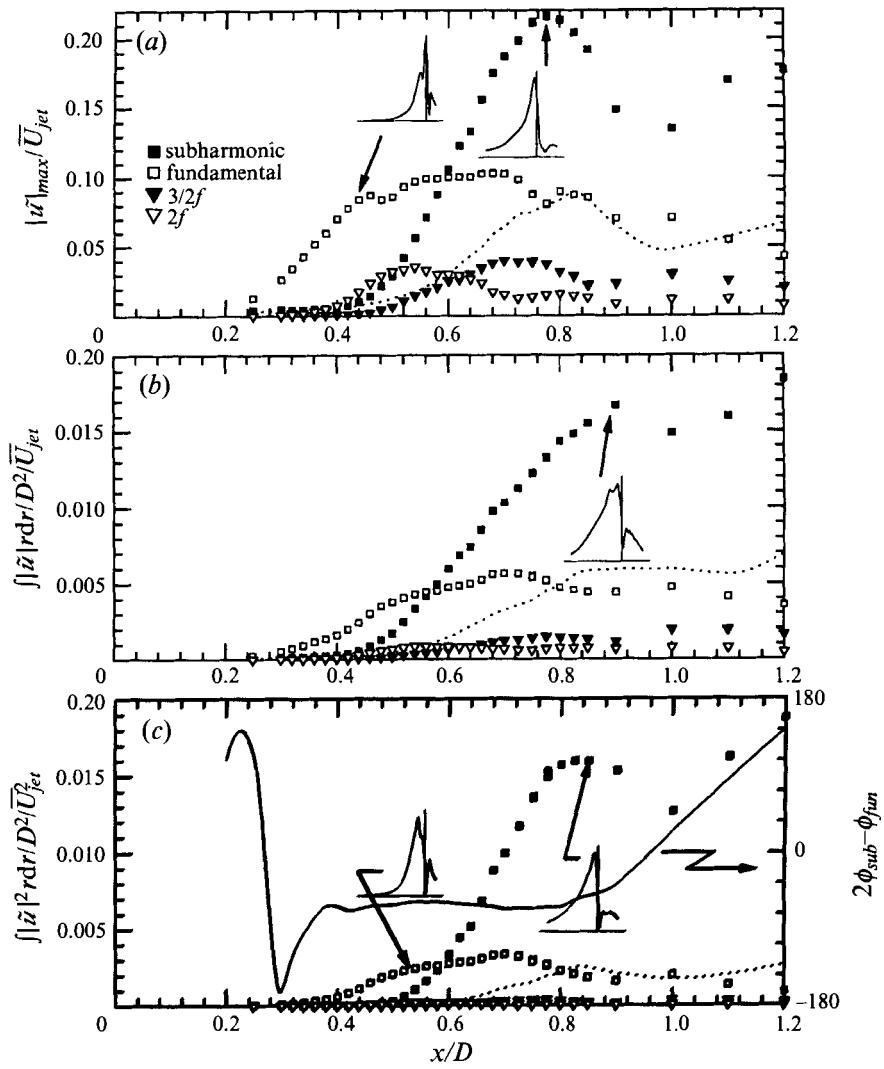

FIGURE 5. Streamwise development of the instability waves (case *III*) presented for different measures. $\Delta\phi = 0°$. (*a*) $\frac{|\tilde{u}|_{max}}{\overline{U}_{jet}}$, (*b*) $\frac{1}{D^2\overline{U}_{jet}}\int_{r=0}^{r_{0.1}}|\tilde{u}^2|rdr$, (*c*) $\frac{1}{D^2\overline{U}_{jet}^2}\int_{r=0}^{r_{0.1}}|\tilde{u}^2|rdr$. The dotted line represents the subharmonic when forced alone, the solid line represents the phase difference $2\phi_{sub} - \phi_{fun}$. The inserts show the radial amplitude distribution at the indicated downstream positions.

onant interaction when prompted by the simultaneous forcing at the two frequencies. The increases in the $\frac{3}{2}f_{fun}$ mode and the first harmonic $2f_{fun}$ with x are substantial, when their evolution is based on considerations of their maximum amplitudes (figure 5*a*). However, the integrated energy contained in these modes is negligible when compared to the energy levels of the subharmonic and the fundamental wave trains (figure 5*a* and figure 5*c*). The maximum amplitudes of the $\frac{3}{2}f_{fun}$ mode keep increasing up to $x/D = 0.7$, while the first harmonic $2f_{fun}$ increases up to $x/D = 0.54$. According to the linear model, the amplification of both waves ($2f_{fun}$ and $\frac{3}{2}f_{fun}$) should have ceased closer to the nozzle. The shear layer becomes neutrally stable to the $\frac{3}{2}f_{fun}$

$\gamma, \Delta\phi$	$\frac{\lvert\tilde{u}_{sub}\rvert_{max}}{\overline{U}_{jet}}$	$\frac{1}{\overline{U}_{jet}D^2}\int_{r=0}^{r_{0.1}}\lvert\tilde{u}_{sub}\rvert r\mathrm{d}r$	$\frac{1}{\overline{U}_{jet}^2D^2}\int_{r=0}^{r_{0.1}}\lvert\tilde{u}_{sub}\rvert^2 r\mathrm{d}r$
$\gamma = 0.1,\ \Delta\phi = 0°$	0.18	0.0132	0.00146
$\gamma = 0.1,\ \Delta\phi = 90°$	0.12	0.0374	0.00012
$M_{90°}/M_{0°}$	67%	28%	8%
$\gamma = 0.4,\ \Delta\phi = 0°$	0.216	0.0154	0.00148
$\gamma = 0.4,\ \Delta\phi = 90°$	0.154	0.0066	0.00036
$M_{90°}/M_{0°}$	71%	43%	24%
$\gamma = 1.6,\ \Delta\phi = 0°$	0.22	0.0172	0.00160
$\gamma = 1.6,\ \Delta\phi = 90°$	0.155	0.0117	0.00080
$M_{90°}/M_{0°}$	70%	68%	50%

TABLE 2. Differences between the maximum level reached for the subharmonic in the amplified case and in the suppressed case for various initial amplitude ratios and various measures.

mode at $x/D = 0.45$ and to the harmonic frequency at $x/D = 0.25$. Both waves are thus amplified nonlinearly, the harmonic frequency is a consequence of the finite amplitude of the fundamental wave while the $\frac{3}{2}f_{fun}$ is tied to the interaction of the fundamental and the subharmonic wave.

The resonance conditions (3.3) and (3.4) are met because the fundamental is neutrally stable at $x/D = 0.53$ (figure 5*c*) and equal phase speeds are attained since the phase difference $(2\phi_{sub} - \phi_{fun})$ remains constant. This phase difference, taken at $\eta = -5$, is plotted as a solid curve in figure (5*c*). It is clearly a constant between $0.4 < x/D < 0.8$.

4. The influence of initial parameters

4.1. *The initial amplitude ratio*

Forcing the jet at two frequencies simultaneously permitted us to assess the significance of the initial phase difference ($\Delta\phi$), the absolute amplitudes, and the relative amplitude ratio ($\gamma = A_{sub}/A_{fun}$) between the two input waves on the growth of the subharmonic. The results obtained for an initial amplitude ratio of $\gamma = 0.4$ (case *IV*) and for four different phase differences, $\Delta\phi$, are shown in figure 6. The subharmonic frequency (figure 6*a*) is amplifying very rapidly beyond $x/D = 0.52$ for all initial phase angles but one at $\Delta\phi = 90°$. This amplification is sustained until $\int \lvert\tilde{u}\rvert^2 r\,\mathrm{d}r/D^2/\overline{U}_{jet}^2$ attains its saturation level which is approximately 0.0015. When the criterion of maximum amplitude (equation (3.7*a*)) is used one can observe that not only was the initial amplification at $\Delta\phi = 90°$ lower than at the other $\Delta\phi$ but in this case the maximum level of $\lvert\tilde{u}\rvert_{max,sub}/\overline{U}_{jet}$ attained was only 0.05 (at $x/D = 0.62$) before the amplitude of the subharmonic got suppressed. This characteristic is less pronounced when the energy criterion (equation (3.7*c*)) is used. This suppression persists until $x/D = 0.68$ whereupon a rapid amplification is realized. Neither the fundamental wave (figure 6*b*) nor its harmonic component (figure 6*c*) are strongly affected by $\Delta\phi$. The fundamental wave saturates initially at $\lvert\tilde{u}\rvert_{max}/\overline{U}_{jet} = 0.09$ which corresponds to $0.42 < x/D < 0.5$ where $St_\theta \approx 0.3$ and where the fundamental wave is no longer amplified linearly. Nevertheless the amplitude and the energy keep increasing up to $x/D = 0.68$ presumably due to the exchange of energy with the subharmonic wave. It

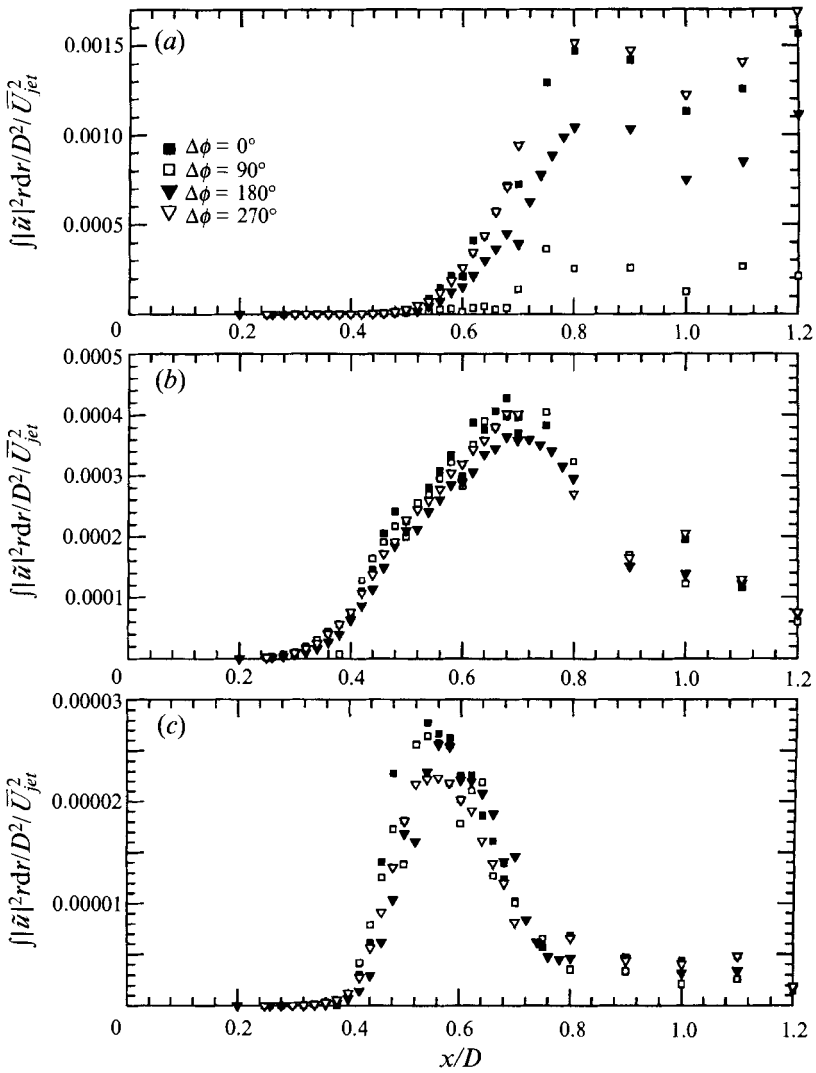

FIGURE 6. The variation of the energy of the different modes with x/D for four different phase angles, $\gamma = 0.4$ (case IV): (*a*) subharmonic, (*b*) fundamental, (*c*) harmonic.

is worth noting that the amplitude and the energy of the fundamental are independent of the amplitude of the subharmonic. The amplitude and energy of the fundamental are of the same order of magnitude as the subharmonic (figures 6*a* and 6*b*) but an order of magnitude larger than the harmonic (figure 6*c*).

In order to determine whether the streamwise suppression of the subharmonic wave depends on the imposed amplitude ratio between the two forced waves (the subharmonic and the fundamental), the experiment was repeated at two additional amplitude ratios of $\gamma = 0.1$ (case V) and $\gamma = 1.6$ (case III) at various initial phase angles. The *overall forcing level was maintained at a constant value* in spite of the different amplitude ratios. The variation of the integrated energy (equation (3.7*c*)) with x/D is displayed in figure 7 for $\gamma = 0.1$ and five different initial phase angles. Once again the lowest amplitude was observed for an initial phase difference of $\Delta\phi = 90°$. The very low forcing level of the subharmonic frequency at $\gamma = 0.1$ is responsible for

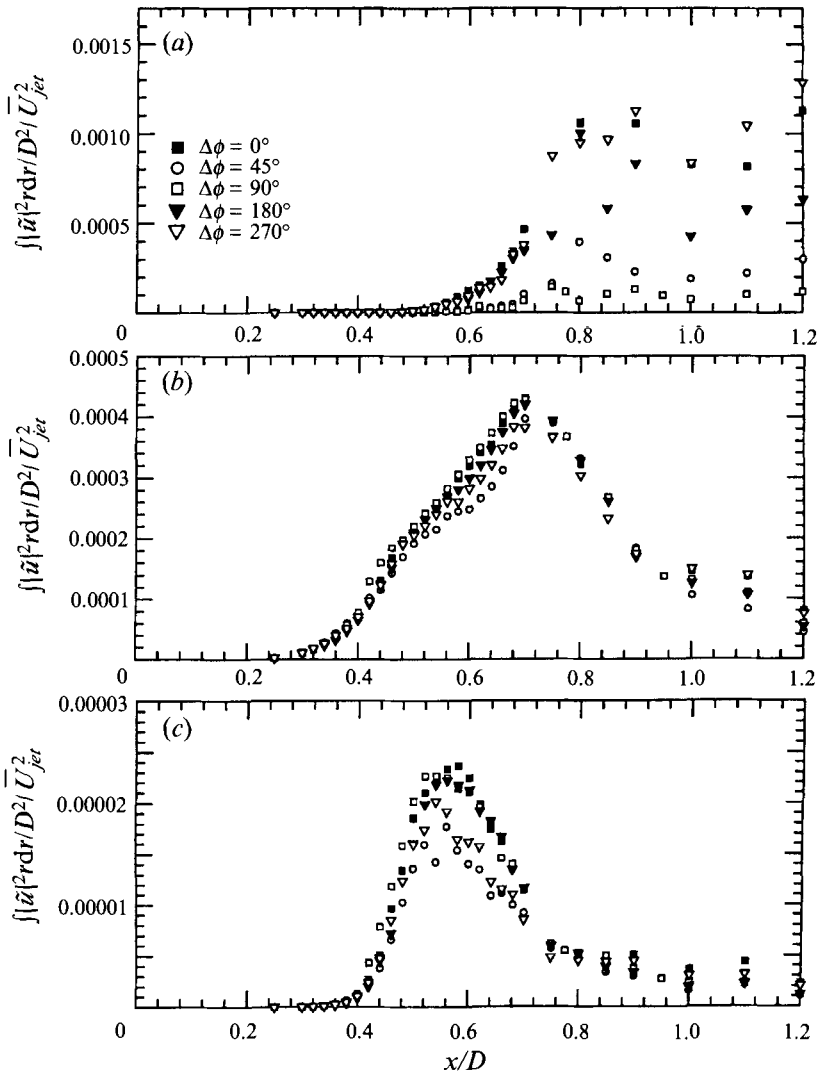

FIGURE 7. The variation of the energy of the different modes with x/D for five different phase angles, $\gamma = 0.1$ (case V): (*a*) subharmonic, (*b*) fundamental, (*c*) harmonic.

the large scatter in the subharmonic data due to a less pronounced coherent motion. Only two values of $\Delta\phi$, 0° and 90°, were considered for $\gamma = 1.6$ (figure 8) as we expected the amplitude of the subharmonic to be smallest for $\Delta\phi = 90°$ which was indeed found to be the case.

The amplitudes of the fundamental and the harmonic waves were insensitive to the changes in $\Delta\phi$, irrespective of γ. Since the momentum thickness θ was not affected by $\Delta\phi$ and γ until the resonant amplification of the subharmonic was well established it is possible to compare the response of the subharmonic to γ for two different initial phase angles directly, one leading to the most suppressed subharmonic ($\Delta\phi = 90°$) and the other one to the most amplified subharmonic ($\Delta\phi = 0°$). The results for the three amplitude ratios $\gamma = 0.1$, 0.4, and 1.6 at $\Delta\phi = 0°$ and 90° are summarized in table 2 using the three different criteria of amplification described in § 3.3. Table 2 displays the importance of choice of criterion used to describe the evolution of an instability

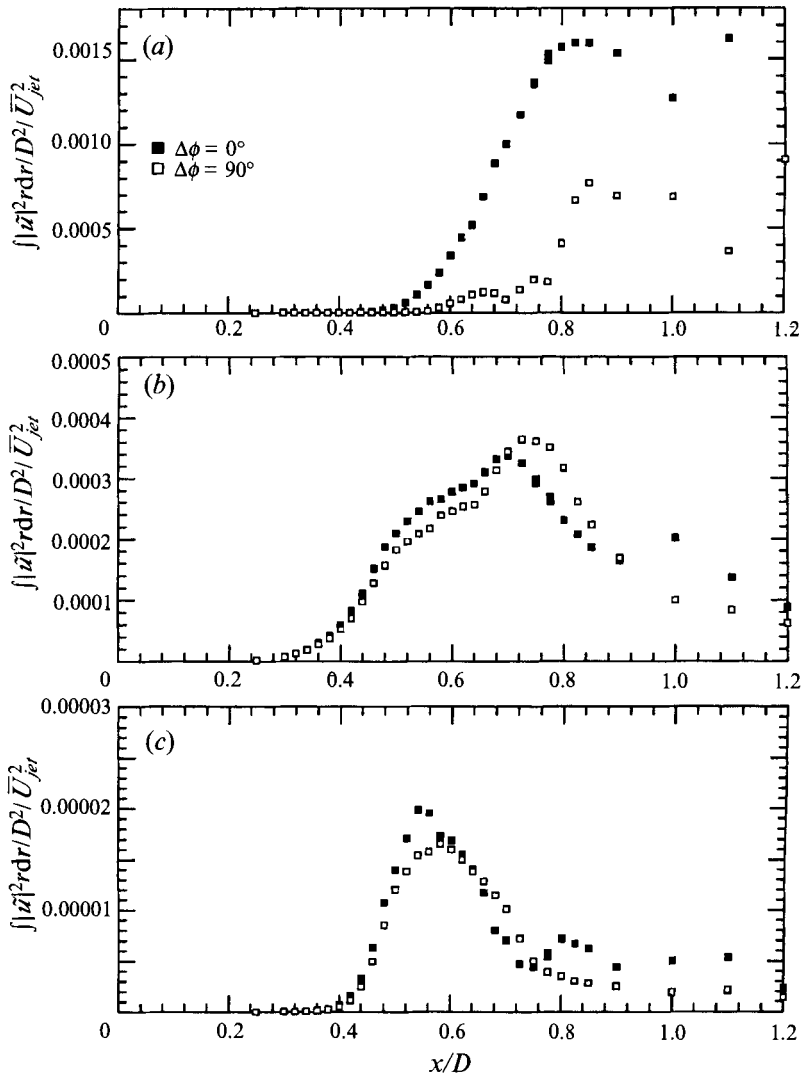

FIGURE 8. The variation of the energy of the different modes with x/D for two different phase angles, $\gamma = 1.6$ (case III): (*a*) subharmonic, (*b*) fundamental, (*c*) harmonic.

wave. It compares the maxima measured at each streamwise location for the case of the suppressed subharmonic ($\Delta\phi = 90°$) and for the most amplified subharmonic ($\Delta\phi = 0°$). The degree of suppression of the maximum amplitude (equation (3.7*a*)) of the subharmonic at $\Delta\phi = 90°$ relative to $\Delta\phi = 0°$ was independent of the initial amplitude ratio. For example, for an initial $\gamma = 0.1$ the maximum amplitude of the suppressed case ($\Delta\phi = 90°$) was 67% of the maximum amplitude in the most amplified case ($\Delta\phi = 0°$), displayed in table 2 by the quantity $M_{90°}/M_{0°}$, where M stands for the different measures (equations (3.7*a–c*)). Both maxima occur at $x/D \approx 0.8$. The ratio, $M_{90°}/M_{0°}$, changed by merely 3% when the imposed γ was increased by a factor of 16 (i.e. to $\gamma = 1.6$) while a constant overall forcing level was maintained. The integral measures (columns 3 and 4 in table 2) are considerably more sensitive to γ. They indicate that the degree of suppression of the subharmonic decreases with increasing

γ. The absolute percentages are not important since the azimuthal resolution of $\Delta\phi$ was only by $\Delta\phi = 90°$.

4.2. *The overall forcing level*

All theoretical models discussed above assume parallel flow and small amplitudes. Raising the total forcing level might violate these assumptions as it leads to nonlinear interactions and to an increase in the spreading rate of the mean flow field. The effect of doubling the amplitude of the combined wave while maintaining $\gamma = 0.1$ (case *VI*) on the integrated energy across the flow is shown in figure 9. Doubling the combined forcing level eliminated the effect of the initial phase difference between $\Delta\phi = 0°$ and $\Delta\phi = 90°$, irrespective of the criterion by which it was assessed (i.e. maximum amplitude or integrated energy). It is possible that the effect of $\Delta\phi$ is found for values in the range $90° < \Delta\phi < 360°$.

Additional measurements were made along the centreline of the jet column at higher forcing levels and three different pairs of frequencies: (*i*) 184/368 Hz (case *VII*), (*ii*) 62/124 Hz (case *VIII*) and (*iii*) 31/62 Hz (case *IX*). The lower frequencies produced a longer fetch in which interaction could be studied. For all three cases $\gamma = 0.1$ while the initial phase-locked forcing level of the fundamental (measured on the centerline at $x/D = 0.2$) changed to $|\tilde{u}_{fun}|/\overline{U}_{jet} = 0.5\%$ for case (*i*), 1.7% for case (*ii*) and 2.7% for case (*iii*). The downstream evolution of the phase-locked amplitudes of the subharmonic along the centreline for case (*i*) is plotted in figure 10*a* for two different $\Delta\phi$. The solid line represents the amplitude of the subharmonic for an initial $\Delta\phi = 0°$, and the dashed line shows the same for $\Delta\phi = 90°$. The maximum amplitude attained with $\Delta\phi = 0°$ is now 93% of the maximum amplitude attained with $\Delta\phi = 90°$ and it occurs approximately $1.8D$ further downstream. Forcing the jet at 62 and 124 Hz results in the same ratio of the maximum amplitudes (figure 10*b*). No resonant amplification was observed for the pair of 31 and 62 Hz, regardless of the initial phase difference. In this case the two waves do not travel with the same phase speed in the region where the mode $m = 0$ is amplified linearly. They have, therefore, no opportunity for a resonant interaction. At large x/D, where the two waves become non-dispersive, only the helical mode $m = 1$ is still linearly amplified. Thus resonance cannot take place. Forcing at high amplitudes renders the amplification of the subharmonic independent of the initial phase difference.

4.3. *The spreading rate of the forced mixing layer*

The spatial stability analysis of an axisymmetric jet suggests that pure suppression of the subharmonic wave is only feasible in parallel flow (Monkewitz 1988). Since the spreading rate of a shear layer forced at high amplitudes is increased, the parallel flow assumption might be invalid. This may inhibit the suppression of the subharmonic wave for some initial phase angles as was indeed observed for case *VI*. To address this question a trip ring was installed inside the nozzle, 25.4 mm upstream from the exit, in order to bring the transition closer to the nozzle exit. Axial notches were cut in the ring to forestall organized vortex shedding on its leeward side. The ring is about 3.6 mm wide and about 0.5 mm thick, which is approximately equal to the thickness of the laminar boundary layer in the nozzle for the velocity range investigated.

The streamwise evolution of the momentum thicknesses and the turbulence intensities for the unexcited flow with and without the trip ring are compared in figure 11. The turbulence intensities, plotted on an arbitrary scale, are initially increased many fold due to the trip ring but the difference vanishes with x and at $x/D \approx 0.84$ the intensities become roughly equal for both cases. Although the momentum thickness

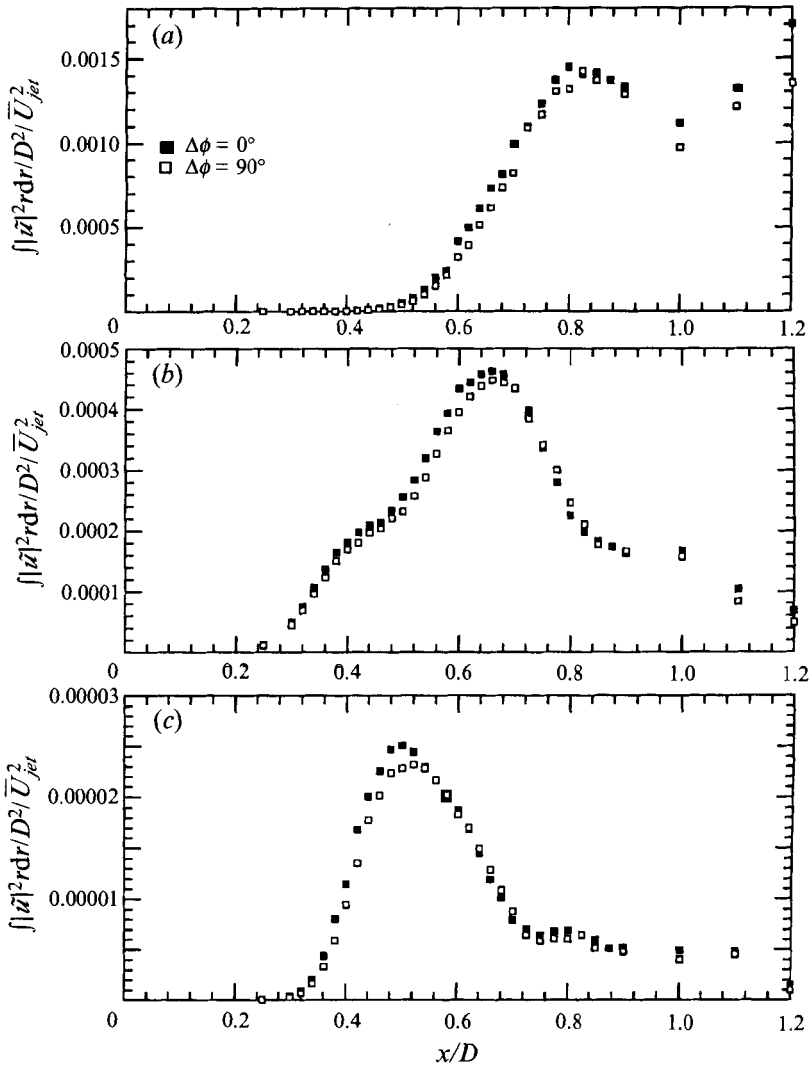

FIGURE 9. The variation of the energy contained in the different modes and the phase with x/D for a higher forcing level (case *VI*) and two different initial phase angles, $\Delta\phi = 0°$, $\Delta\phi = 90°$, $\gamma = 0.1$; (*a*) subharmonic, (*b*) fundamental, (*c*) harmonic.

was increased by approximately 25% between $0.5 < x/D < 0.75$ (the region in which a resonant interaction was deemed to occur) as a consequence of the upstream movement of the transition location from $x/D = 0.5$ to $x/D = 0.3$, the rate of spread of the turbulent shear layer was not altered (figure 11). Resonant interaction occurred at $x/D > 0.5$ independently of the trip ring, and the rate of growth of the subharmonic was strongly coupled with the initial phase difference (figure 12). In this case the resonance was suppressed at an initial phase difference of $\Delta\phi = 0°$ in contrast to case *III* where suppression occurred at $\Delta\phi = 90°$. The trip ring shifted the resonant interaction by a quarter wavelength, $\lambda/4$, upstream because it increased the local width of the basic flow by approximately 25% in the region where the interaction occurred. It appears (figure 11) that the enhanced background turbulence has only a marginal effect on the resonant interaction and the generation of the subharmonic

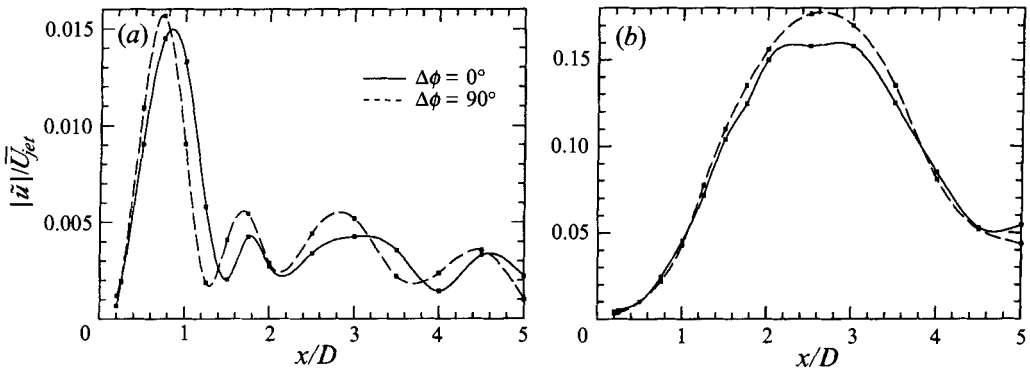

FIGURE 10. The variation of the amplitudes of the subharmonic along the centreline with x/D for a higher forcing level and two different initial phase angles: (*a*) f_{fun} = 368 Hz, f_{sub} = 184 Hz, $|\tilde{u}|_{0,fun} = 0.5\%$ (case *VII*); (*b*) f_{fun} = 124 Hz, f_{sub} = 62 Hz, $|\tilde{u}|_{0,fun} = 1.7\%$ (case *VIII*).

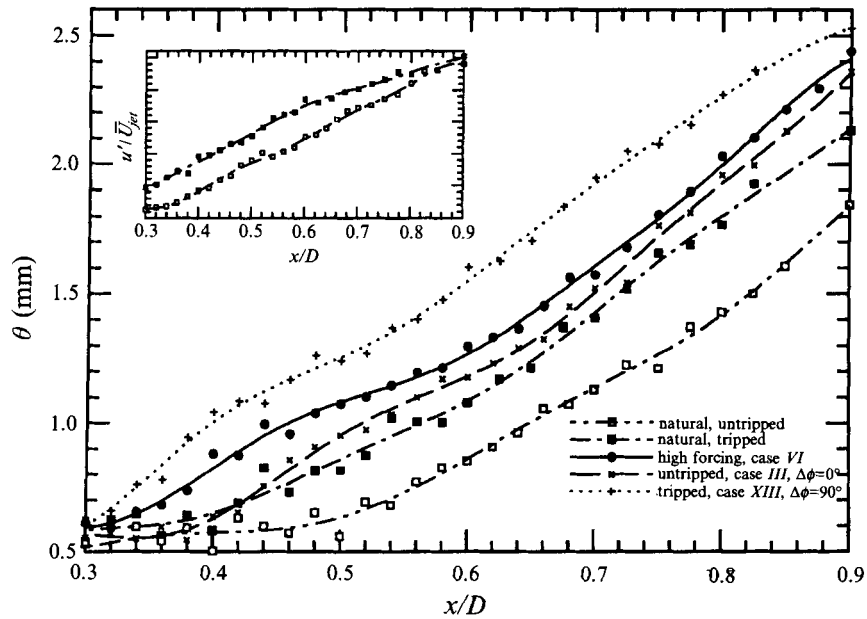

FIGURE 11. The evolution of the momentum thickness and the maximum turbulence intensity along x/D with and without a trip ring.

wave. The observed shift is essentially related to the shift in the virtual origin caused by the trip ring. It is also clear that a strong amplification of the subharmonic wave is coupled with an increase in thickness of the shear layer. External excitation (case *XIII*) of the tripped flow increased the momentum thickness at $x/D = 0.5$ by almost 50% and comparable excitation in the absence of tripping (case *III*) resulted in a similar relative increase in θ at this streamwise location. The local disparity in width between the two basic states (tripped and non-tripped) was retained in spite of the excitation at $\gamma = 1.6$ although the absolute initial-perturbation levels were notably different ($|\tilde{u}|_{max}/\overline{U}_{jet}|_{x/D=0.25} = 1.6\%$ for case *III* while it is 6.5% for case *XIII* – see table 1).

The high forcing level of 3.2% (case *VI*), whose θ value is also plotted in figure 11,

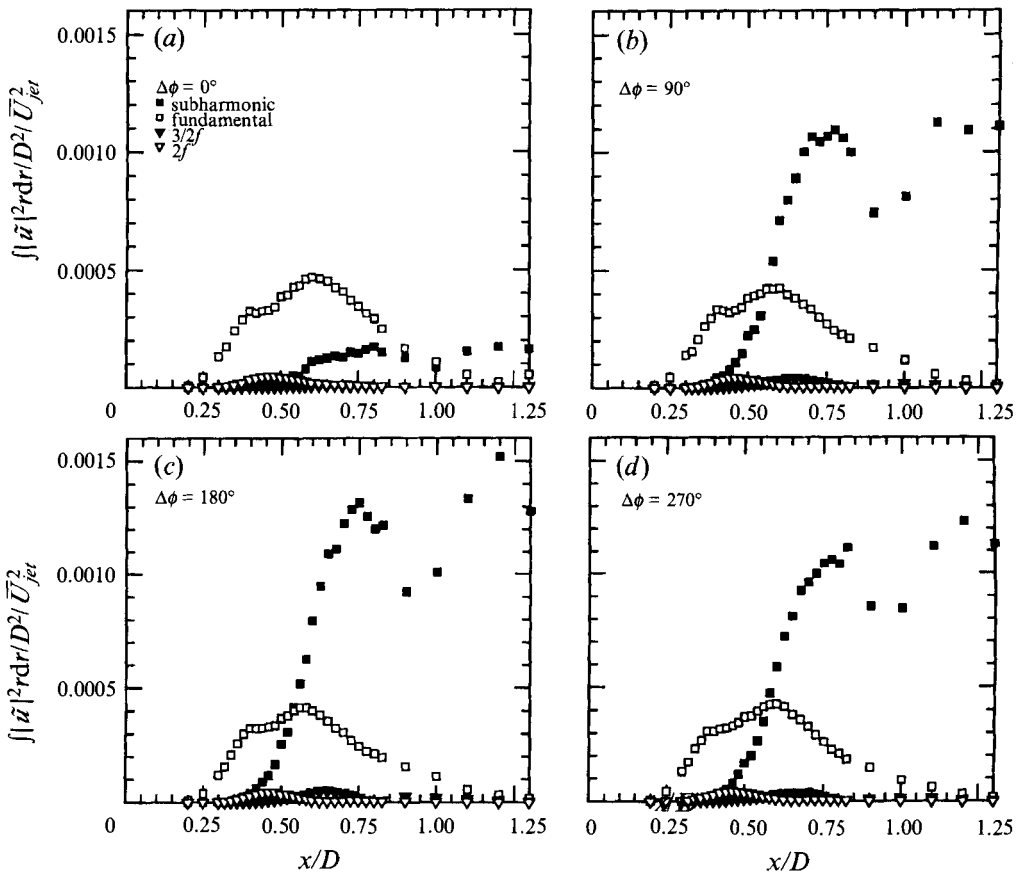

FIGURE 12. The variation of the energy contained in the different modes with x/D for the tripped nozzle and four different initial phase angles (case *XIII*).

produced a local momentum thickness which is between that of the highly amplified results of cases *III* and *XIII* from $x/D = 0.3$ onwards. Since there is an initial phase shift of approximately 90° for the two subharmonic interactions occurring in cases *III* and *XIII*, the intermediate θ associated with case *VI*, which was excited at the same frequencies as cases *III* and *XIII*, may necessitate a 30° – 45° phase shift to suppress the growth of the subharmonic. Since data at this $\Delta\phi$ were not measured the association of the lack of suppression with the high amplitude of forcing remains uncertain. It may be surmised that the initial $\Delta\phi$ required for suppression of the subharmonic depends on the initial thickness at which resonant interaction is to occur.

4.4. *The forcing frequency*

The streamwise location of the interaction between the subharmonic and fundamental depends on the local Strouhal number $St_\theta = \omega\theta/\overline{U}_{jet}$ and thus for a given Reynolds number $Re_D = D\overline{U}_{jet}/\nu$ and jet velocity it depends on the forcing frequency. For a lower Strouhal number the two waves will have the same phase speed and maximum growth rate further downstream provided $\theta(x)$ will not be significantly altered (see figures 1*a* and 1*b*). Data were taken at various streamwise locations up to 2 nozzle

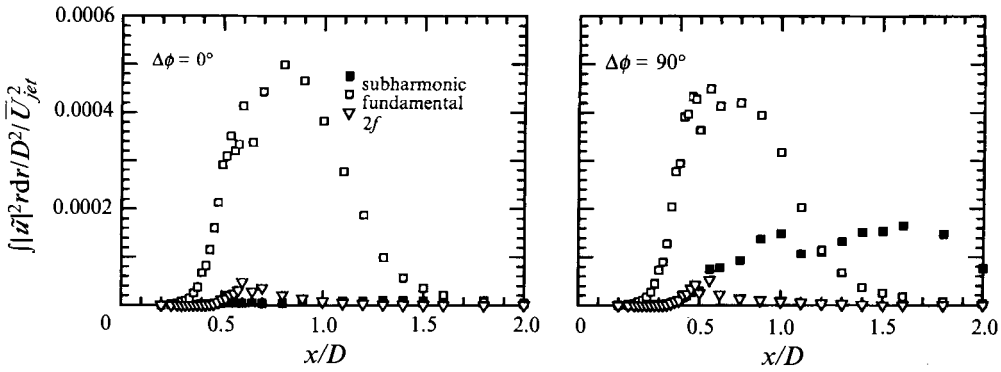

FIGURE 13. The variation of the energy with x/D for a frequency pair of $f_{sub} = 140$ Hz and $f_{fun} = 280$ Hz (case XIV) for two different initial phase angles.

diameters for two additional frequency pairs. The influence of two initial phase angles ($\Delta\phi = 0°$ and $\Delta\phi = 90°$) was investigated. The initial amplitude ratio was $\gamma = 1.6$.

The results for a frequency pair of $f_{sub} = 140$ Hz and $f_{fun} = 280$ Hz (case XIV) are displayed in figure 13. Here the subharmonic was only slightly amplified for an initial phase difference of $\Delta\phi = 90°$. It reached its maximum energy for the first time at $x/D = 1.0$ and later at $x/D = 1.6$. At both locations, however, the integrated energy of the subharmonic was only 30% of the fundamental rather than being 3 times larger than the fundamental as, for example, for case V. It should be noted that the amplitude of the fundamental in those two cases (XIV and V) was not much different. For an initial phase difference of $\Delta\phi = 0°$ the subharmonic was suppressed. A strong subharmonic could be observed for a frequency pair of $f_{sub} = 150$ Hz and $f_{fun} = 300$ Hz (case XV) at an initial phase difference of $\Delta\phi = 0°$ (figure 14). In this case an initial phase difference of $\Delta\phi = 90°$ leads to suppression of the subharmonic as it happened in cases III–V which were forced at higher frequencies of 184 and 368 Hz. The maximum integrated energy of the subharmonic wave in this case was only 0.001 at $x/D = 0.8$ in comparison to 0.0016 for case III (figure 5). Thus, there is a *progressive* deterioration by a factor of 3 in the maximum amplitude attained as the subharmonic frequency is reduced from 184 to 140 Hz at $\Delta\phi = 0°$. This suggests that the resonant enhancement of the subharmonic is frequency dependent. Different frequency pairs also respond differently to the initial phase angle – leading to either amplification or suppression of the subharmonic wave train. The less pronounced gain of energy of the subharmonic for the frequency pair 140–280 Hz might be in part also due to the coarse step in $\Delta\phi$ and the high levels of random turbulence existing farther downstream decreasing the interaction of the instability waves at the investigated low forcing level.

4.5. *Slightly non-matching resonance conditions*

Another feature of subharmonic resonance is the excitation of sidebands around the subharmonic frequency, when forcing with a detuned frequency $\omega_{det} = \omega_{sub} \pm \Delta\omega$. By superposing the detuned subharmonic and the fundamental waves in an amplitude modulated forcing signal, with a continuous change of $\Delta\phi$, the resonance conditions predict the generation of a second sideband $\omega_{out} = \omega_{fun} - \omega_{det}$ which is symmetrical about the subharmonic frequency (Monkewitz 1988). The demand for equal phase speed changes under detuned forcing to $c_{ph,out} = c_{ph,fun}(1 \mp \Delta\omega/\omega_{sub})$, which can be reduced to $c_{ph,out} = c_{ph,fun}$ for a small detuning $\Delta\omega$.

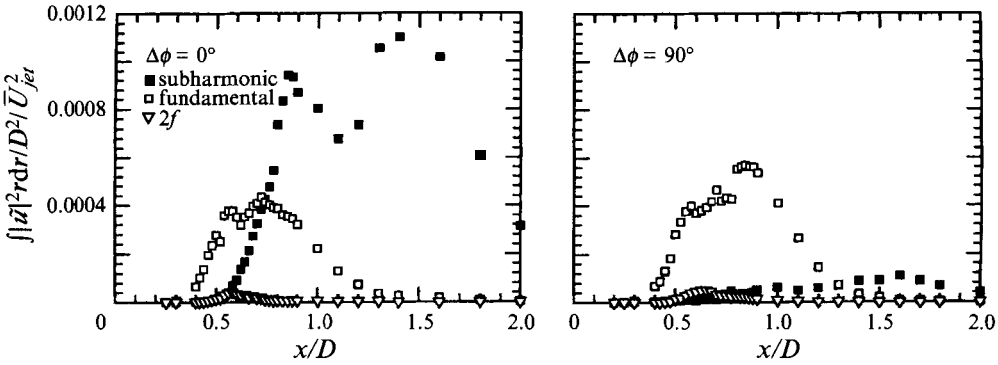

FIGURE 14. The variation of the energy with x/D for a frequency pair of $f_{sub} = 150$ Hz and $f_{fun} = 300$ Hz (case XV) for two different initial phase angles.

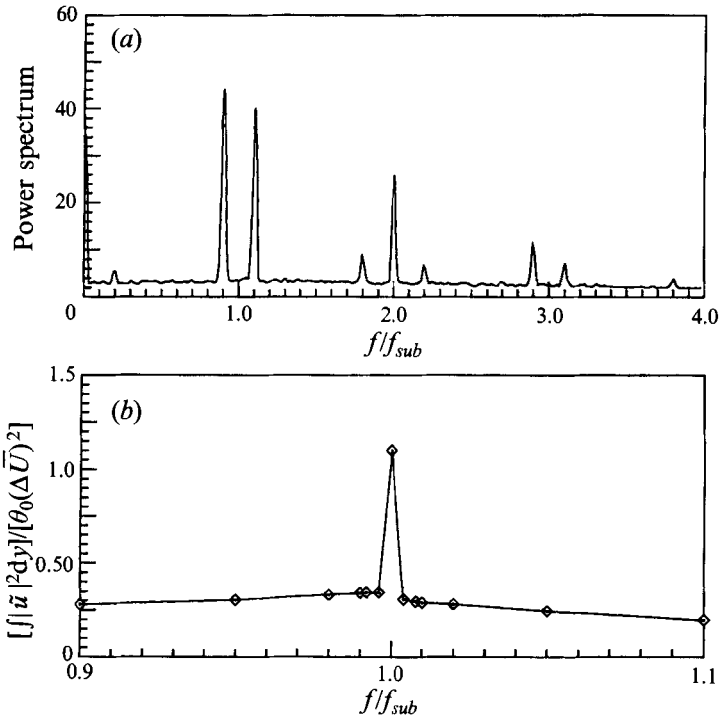

FIGURE 15. (*a*) Power spectrum taken at the downstream location where $E_{max} = \int \tilde{u}_{sub} dy = \max$ for a detuning frequency $\Delta f = 10\%$. (*b*) Energy of the subharmonic at the streamwise location of $E_{sub,max}$ for different detuning frequencies Δf: subharmonic and sidebands.

The power spectrum shown in figure 15(*a*) was measured in a plane mixing layer at the downstream location where the energy of the subharmonic is at its maximum. It shows the generation of a second sideband $\omega_{out} = \omega_{fun} + \omega_{det}$ for $(\omega_{det} - \omega_{sub})/\omega_{sub} = -10\%$. It does not indicate a strong dependence of the magnitude of the spectral peak of the sidebands on the detuned frequency investigated. The precise occurrence of an instability wave at the subharmonic frequency was not observed. Less energy is contained in the sidebands (figure 15*b*) than in the case when the forcing is precisely at the subharmonic frequency. It shows, however, only a weak

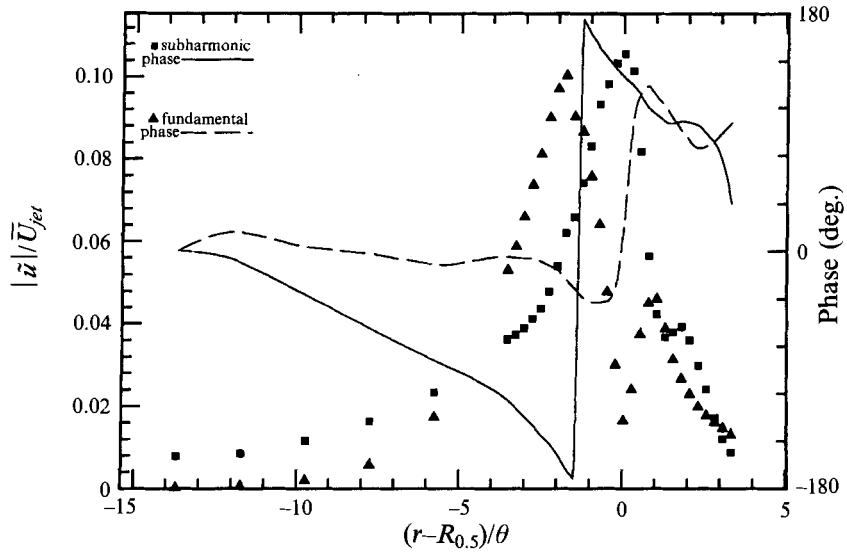

FIGURE 16. Lateral distribution of normalized amplitudes and phases of the subharmonic and the fundamental at $x/D = 0.6$, $\gamma = 1.6$ (case *III*)

dependence on the detuning frequency $\Delta\omega$. When one sideband is forced one may observe the emergence of a resonant sideband which is symmetric with respect to the subharmonic frequency, the energy is supplied to two instability waves instead of to the one resonant subharmonic.

5. Resonance conditions and initial phase difference

Michalke (1984) and Cohen & Wygnanski (1987*b*) showed theoretically that for subharmonic resonance to occur two conditions (i) $\alpha_{i,fun} = 0$ and (ii) $c_{ph,fun} = c_{ph,sub}$ have to be satisfied. It was shown earlier that the initial phase difference between the two instability waves has to be considered as it may strongly influence the development of the subharmonic. The condition of equal phase speed is equivalent to the condition that

$$2\phi_{sub} - \phi_{fun} = \text{const}, \tag{5.1}$$

where ϕ is the phase of either wave. For resonance a constant phase difference between the two waves must be maintained in the non-dispersive region depending on the initial $\Delta\phi$ between the two forced waves. Experiments showed that the initial location where ($2\phi_{sub} - \phi_{fun} = \text{const}$) depends on $\Delta\phi$ and consequently the resonance between the waves might be inhibited. In a divergent mixing layer the phase speed is not constant across the shear layer (e.g. Gaster *et al.* 1985) and thus the equality of phase speeds at one radial location might be misleading. In addition the phase varies across the mixing layer (figure 16). Fortunately, the phase angle of the fundamental is almost independent of r on the high-speed side of the flow.

In order to determine the radial and streamwise locations of equal phase speed of the fundamental and the subharmonic, contour plots of the phase difference ($2\phi_{sub} - \phi_{fun}$) were used. The contours of the phase difference as well as the contours of the amplitudes of the subharmonic are displayed for case *III* in figure 17 for $\Delta\phi = 0°$ and $\Delta\phi = 90°$. Horizontal lines (i.e. parallel to the x-axis) in the *phase difference contour plot* (figure 17*a,c*) indicate regions where the phase velocities of

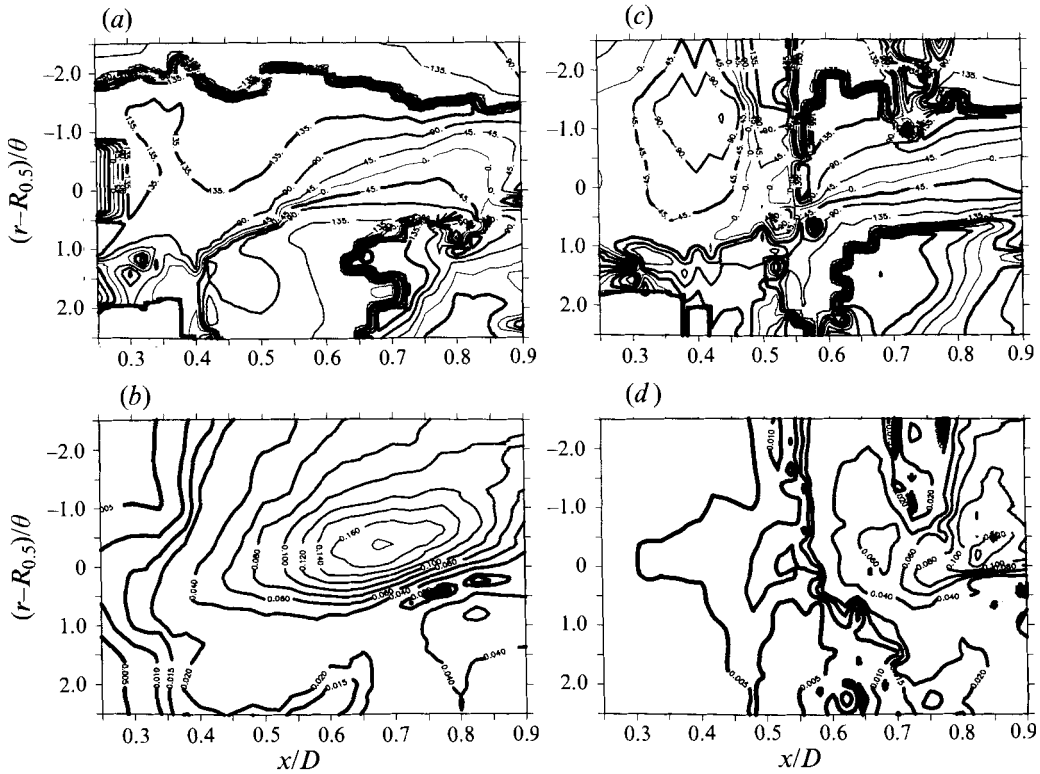

FIGURE 17. Contours of the amplitudes and phase difference ($2\phi_{sub} - \phi_{fun}$) for case *III*: (*a*) phase difference $\Delta\phi = 0°$, (*b*) amplitude $\Delta\phi = 0°$, (*c*) phase difference $\Delta\phi = 90°$ and (*d*) amplitude $\Delta\phi = 90°$.

the two waves are identical thus allowing a subharmonic resonance. Vertical lines imply that no resonance is possible since the dispersiveness of the waves is largest. The distances between the contours in the *amplitude contour plot* (figure 17*b*, *d*) are inversely proportional to the spatial amplification rate.

In the case of the amplified subharmonic (figure 17*a*, *b*) the strongest amplification takes place near the centre of the shear layer. The maxima of the amplitudes of the subharmonic wave occur on the high-speed side of the centreline, in agreement with the observations of Cohen & Wygnanski (1987*a*). The thick horizontal line in the phase contour plot (figure 17*a*) starting at $(r - R_{0.5})/\theta \approx -2$ depicts the phase reversal occurring at this radial location over all the stations considered (approximate phase shift of π). Another phase reversal in the streamwise direction appears at $x/D = 0.65$ between $2.5 > [(r - R_{0.5})/\theta] > 0.5$. The strongly amplified region of the subharmonic resides between those phase-reversal curves. The streamwise (vertical) phase reversal is accompanied by a rapid reduction in amplitude of the subharmonic. The strongest region of amplification occurs between $-45° < (2\phi_{sub} - \phi_{fun}) < 135°$, i.e. over the 180° of the subharmonic wave where the amplitude of the subharmonic is enhanced. Along with the maximum amplitude, the line of zero phase difference is inclined towards the inner side of the jet with increasing x, i.e. the two waves near the centre of the mixing layer maintain their favourable phase difference providing optimal phase locking. Furthermore, for all the initial phase differences examined, the two interacting waves switched to an initial phase difference of $\Delta\phi = 0°$ at the radial

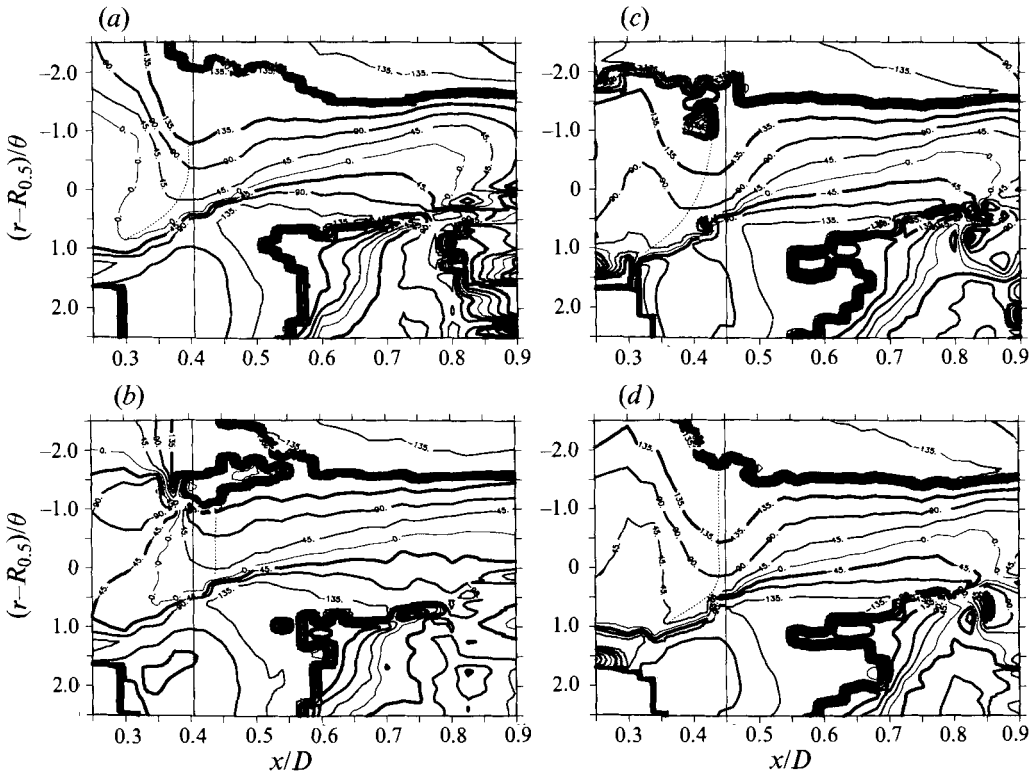

FIGURE 18. Contours of the phase difference $(2\phi_{sub} - \phi_{fun})$: (*a*) tripped nozzle (case *XIII*), $\Delta\phi = 90°$ (amplified subharmonic), (*b*) tripped nozzle (case *XIII*), $\Delta\phi = 0°$ (suppressed subharmonic), (*c*) higher forcing level (case *VI*) $\Delta\phi = 0°$, (*d*) higher forcing level (case *VI*) $\Delta\phi = 90°$.

location of highest amplitudes. Thus the radial location of the favourable interaction is significant.

In the case with suppressed resonance ($\Delta\phi = 90°$) phase locking between subharmonic and fundamental sets in much further downstream at $x/D \approx 0.6$ (figure 17*c*). The amplitude contour plot of the subharmonic wave (figure 17*d*) indicates no significant gain up to $x/D = 0.6$ but increasing amplitudes downstream of this point. The phase difference contour plots (figure 17*c*) show constant phase differences $(2\phi_{sub} - \phi_{fun})$ between the two waves starting from $x/D > 0.6$ in the central core of the shear layer. This occurs after the streamwise phase reversals which are at $x/D \approx 0.53$ on the high-speed side of the jet and at $x/D \approx 0.6$ on the low-speed side of the flow. Thus the radial region in which the phase of the subharmonic is linked to the phase of the fundamental is limited to $-1 < (r - R_{0.5})/\theta < 0.5$. For this reason the interaction between the two waves is inhibited and no subharmonic enhancement could be achieved up to $x/D \approx 0.6$. Only in a small region around $-0.5 < (r - R_{0.5})/\theta < +0.5$ and $x/D > 0.6$ are the waves non-dispersive and a small gain in the subharmonic amplitude can be observed. The absolute maximum of the subharmonic occurs farther downstream in comparison to the amplified case, due to the late interaction and the reduced growth rate of the shear layer.

The cases of the tripped nozzle (case *XIII*) and the higher amplitude forcing (case *VI*) are of special interest. Both cases have comparable strong growth rates of the subharmonic wave but at the higher forcing amplitudes the influence of $\Delta\phi$ vanished

for $\Delta\phi = 0°$ and 90° while for the tripped nozzle flow the effect of $\Delta\phi$ reversed itself relative to the case for which transition occurred naturally requiring $\Delta\phi = 90°$ for amplification and $\Delta\phi = 0°$ for suppression. In this case the contour plots showing the phase difference are similar regardless of the amplification rate of the subharmonic (figure 18*a*, *b*). However, in the initial region of a subharmonic interaction (i.e. around $x/D \approx 0.4$), where the fundamental wave ends its amplification, differences in the phase contours are noted. The dotted line in these plots indicates the initial position from which the two waves become non-dispersive. The straight vertical solid line marks the position where the fundamental wave is neutral according to a linear theory. Here the growth rate can be considered as being small, even if the fundamental continues to amplify until it saturates nonlinearly. For the amplified subharmonic case ($\Delta\phi = 90°$) both resonance conditions (stipulated in equations (3.3) and (3.4)) are satisfied (figure 18*a*), while in the suppressed subharmonic case ($\Delta\phi = 0°$) the waves start to be non-dispersive approximately $0.05D$ farther downstream (figure 18*b*). There is also an 'island' of phase reversal which extends from $x/D = 0.4$ to $x/D = 0.55$ around $(r - R_{0.5})/\theta = -1.5$. This is roughly the radial location where the fundamental has its largest amplitude (figure 16). Thus, by changing its phase it may not fulfil its role as a catalyst in the subharmonic growth.

The phase difference contour plots for the highly forced jet (case *VI*) are more similar for $\Delta\phi = 0°$ (figure 18*c*) and $\Delta\phi = 90°$ (figure 18*d*) than the pair of contour plots generated for the tripped flow. Here the subharmonic is amplified irrespective of the initial phase difference investigated. The stronger forcing moves the location of the phase locking of the two waves further upstream irrespective of the imposed $\Delta\phi$. This effect is perhaps responsible for the reduced influence of the initial phase angle. Furthermore there is hardly a region in which phase reversal occurs. No decrease in the wave↔wave interaction in favour of the mean-flow↔wave energy transfer has been observed so far (figure 26) in contradiction to the proposition by Mankbadi (1991) to explain the decreasing influence of the initial phase angle on the resonant interaction when the forcing level is increased.

6. Energy transfer to the resonant waves

6.1. *Energy of the mean flow*

The experimental results obtained for different inflow conditions suggest that a major part of the energy of the subharmonic is supplied by the mean flow. Major differences in the subharmonic energy caused by changing the initial phase angles relative to the fundamental had only a marginal effect on the fundamental itself. The fundamental wave therefore only facilitates the energy transfer to the subharmonic. This observation seems to corroborate the predictions of Orszag & Patera (1983) who showed that in a boundary layer, a direct fundamental–subharmonic energy exchange can only compensate the viscous dissipation in the subharmonic wave.

The Reynolds stress and the production of turbulence (or other oscillatory motion) is related to the mean momentum equation and to the mean kinetic energy equation. Therefore, an increase in the momentum thickness results in a depletion of mean energy of the flow. A rapidly amplifying subharmonic wave causes even further increase of the momentum thickness. This effect is demonstrated in figures 19(*a*) and 19(*b*) for the natural (case *III*) and for the tripped flow (case *XIII*) respectively. The rapidly amplifying subharmonic leads to an increase in the momentum thickness in

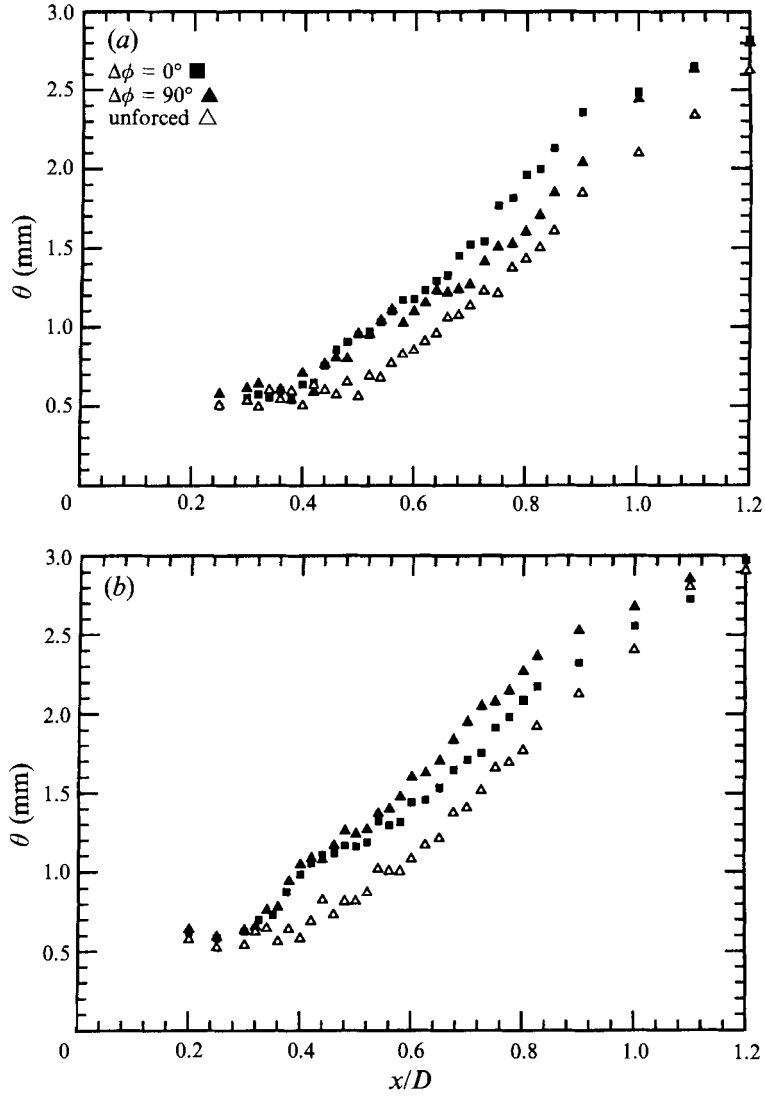

FIGURE 19. Variation of the momentum thickness with x/D: (*a*) case *III* (natural transition), (*b*) case *XIII* (tripped).

the direction of streaming from $x/D = 0.56$ in the natural case (figure 19*a*) and from $x/D = 0.50$ in the tripped case (figure 19*b*).

6.2. *Kinetic energy*

The energy transfer to the subharmonic can be divided into a linear mechanism, described by a linear stability model, and an interaction, which can be further subdivided into a resonant interaction and into other nonlinear mechanisms. The fact that the fundamental, phase-locked fluctuations are not altered by the rapidly growing resonant subharmonic fluctuations, can be attributed to a 'parametric' energy transfer mechanism. In a case of 'parametric' resonance, the growth of the subharmonic wave is decoupled from the fundamental (Kelly 1967) and most of the energy is supplied by the mean flow. The mean flow is assumed to be an infinite source of

kinetic energy as long as it remains parallel. In a typical nonlinear interaction on the other hand, an energy transfer takes place, between any two waves after they attain a finite amplitude. In order to define the mode of energy transfer the kinetic energy contained in the mean flow, the coherent primary motion (assumed to be the phase-locked subharmonic, fundamental and harmonic wave), and in the incoherent turbulence was calculated for the three major cases *III*, *VI* and *XIII* as listed in table 1. For each case, a comparison is made between an amplified and a suppressed subharmonic, whenever a suppression was found.

The kinetic energy contained in the incompressible mean flow at any x-location may be defined as

$$E_{mean} = \int_{r=0}^{r_{0.1}} \overline{U}^3 r \, \mathrm{d}r, \tag{6.1}$$

where $r_{0.1}$ refers to the position at the outer edge of the mixing layer where $\overline{U} = 0.1\overline{U}_{jet}$. The kinetic energy of each wave is then

$$E_{wave} = \int_{r=0}^{r_{0.1}} \overline{U}\,\overline{\tilde{u}^2} r \, \mathrm{d}r = \frac{1}{2}\int_{r=0}^{r_{0.1}} \overline{U}|\tilde{u}|^2 r \, \mathrm{d}r, \tag{6.2}$$

while the kinetic energy of the incoherent turbulence is

$$E' = \int_{r=0}^{r_{0.1}} \overline{U}\,\overline{u'^2} r \, \mathrm{d}r. \tag{6.3}$$

The total fluctuating component, which is usually measured, consists of random turbulence as well as of the coherent motion, which in an externally excited flow is locked in phase with the excitation signal, i.e.

$$(\overline{u_t'^2})^{1/2} = (\overline{u'^2} + \sum_n \overline{\tilde{u}_n^2})^{1/2} \quad (n = \tfrac{1}{2}f_{fun}, f, \tfrac{3}{2}f, 2f \ldots).$$

Since only the streamwise component of the velocity fluctuations was measured in the present experiment, we shall try to use the available information to assess the energy gained or lost by each component and thus to obtain a detailed energy balance.

The respective energy exchange among the mean, the coherent and the turbulent motion was assessed by integrating the kinetic energy over a certain part in the streamwise direction. The principle is demonstrated in figures 20 and 21 by marking the areas of the flow from which these integrals were obtained by hatched lines.

The results are summarized in table 3. The following cases were considered:

(i) Case *XIII* (tripped flow), $\Delta\phi = 0°$ and $\Delta\phi = 90°$. Kinetic energy integrated between $0.45 \leqslant x/D \leqslant 0.6$, figure 20.

(ii) Case *III*, $\Delta\phi = 0°$ and $\Delta\phi = 90°$. Kinetic energy integrated between $0.54 \leqslant x/D \leqslant 0.725$ and $0.775 \leqslant x/D \leqslant 0.9$, figure 21.

(iii) Case *VI* (high forcing), $\Delta\phi = 0°$ and $\Delta\phi = 90°$. Kinetic energy integrated between $0.5 \leqslant x/D \leqslant 0.66$.

The magnitude of the streamwise integrated kinetic energy terms (table 3) for the amplified and the suppressed cases confirms the supposition that most of the energy gained by the subharmonic is supplied by the mean flow.

For the tripped nozzle flow excited simultaneously by two waves (case *XIII*, figure 20) at an initial $\Delta\phi = 0°$, the increase in subharmonic energy was similar to that in the jet forced only at the subharmonic frequency. Comparison of the integrated kinetic energy between the suppressed and the amplified cases for the subharmonic, i.e. $\Delta\phi = 0°$ and $\Delta\phi = 90°$, shows a gain of the amplified subharmonic

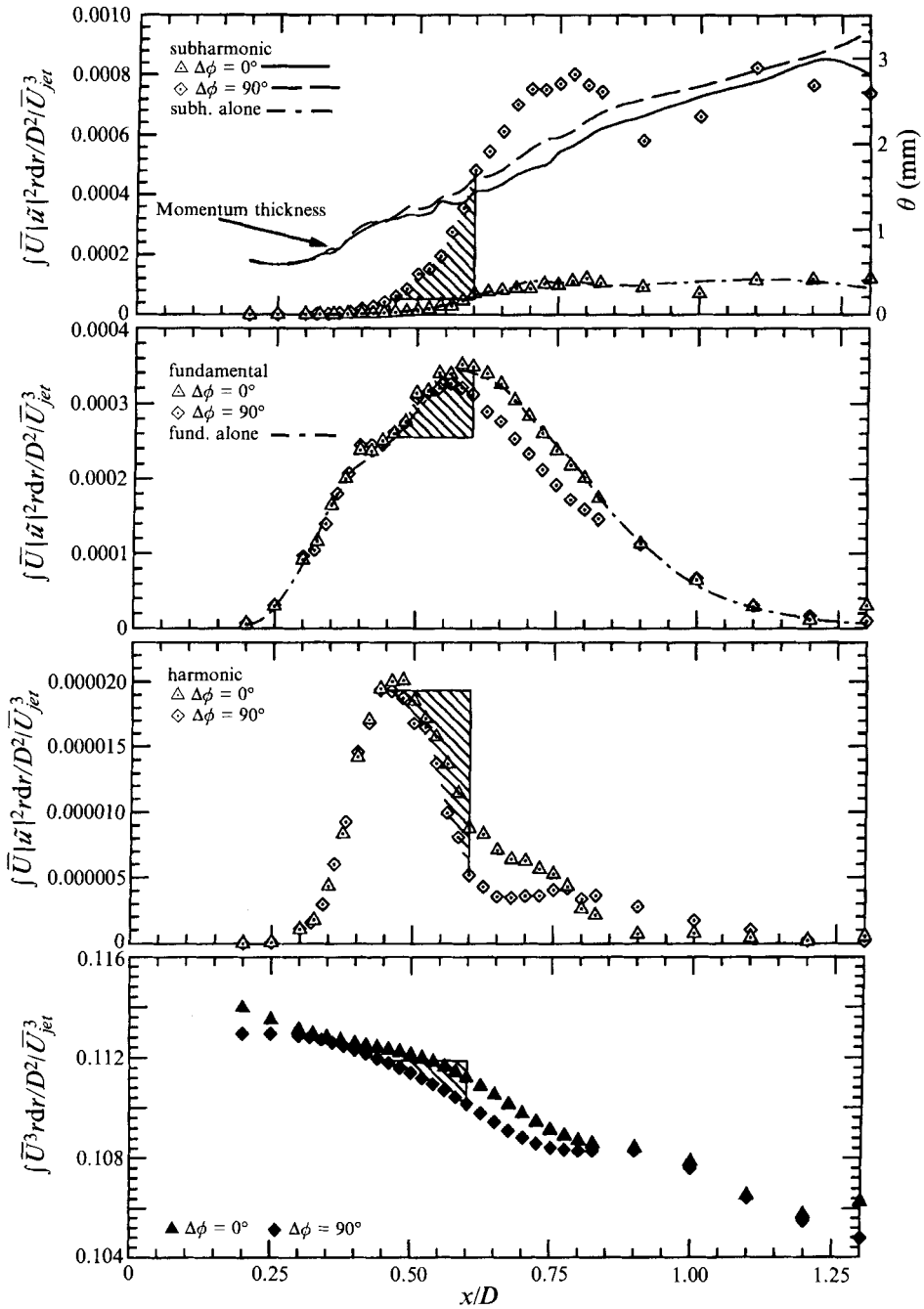

FIGURE 20. Evolution of the kinetic energy integrals with x/D, f_{sub} = 184 Hz, f_{fun} = 368 Hz, tripwire (case *XIII*).

of $\Delta E_{sub} = \int E_{sub,90°} - \int E_{sub,0°} = 0.50$ and a loss in the amplitude of the fundamental of $\Delta E_{fun} = -0.03$. The fundamental seems therefore to contribute only 6% of the gain of the subharmonic in the region investigated. Most of the additional kinetic energy gain stems from the mean motion $\Delta E_{mean} = -2.1$.

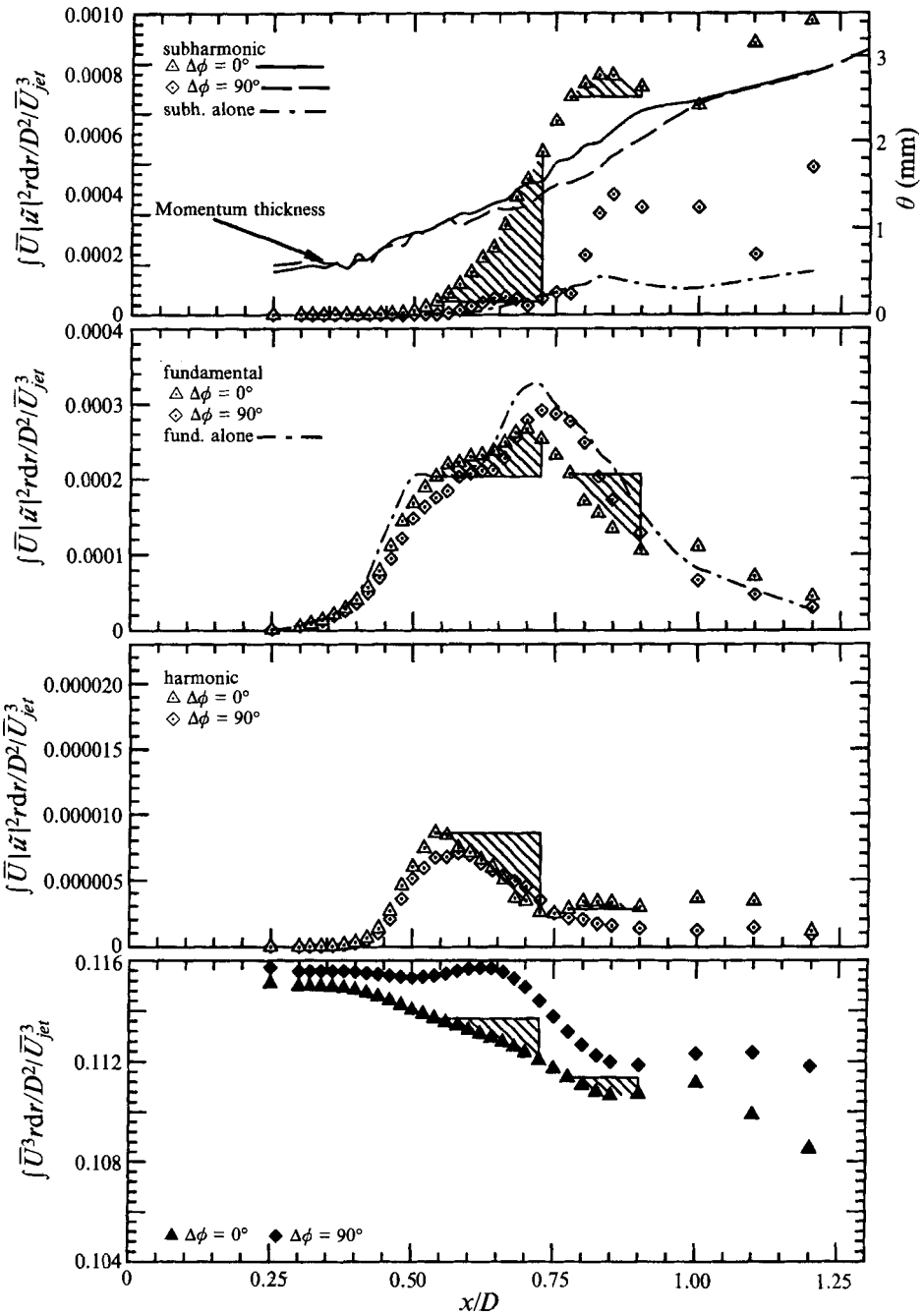

FIGURE 21. Evolution of the kinetic energy integrals with x/D, $f_{sub} = 184$ Hz, $f_{fun} = 368$ Hz (case *III*).

In the non-tripped flow (case *III*) the differences between the amplified and the suppressed subharmonic energy are larger than in the tripped nozzle flow. When $\Delta\phi = 90°$ (the suppressed case) the subharmonic energy does not exceed the level achieved with single periodic forcing at the subharmonic frequency up to $x/D = 0.775$.

Case	$\frac{\int_{x_1}^{x_2} E_{mean}\,dx}{D^3\overline{U}_{jet}^3 \times 10^3}$	$\frac{\int_{x_1}^{x_2} E_{sub}\,dx}{D^3\overline{U}_{jet}^3 \times 10^3}$	$\frac{\int_{x_1}^{x_2} E_{fun}\,dx}{D^3\overline{U}_{jet}^3 \times 10^3}$	$\frac{\int_{x_1}^{x_2} E_{har}\,dx}{D^3\overline{U}_{jet}^3 \times 10^3}$	$\frac{\int_{x_1}^{x_2} E'dx}{D^3\overline{U}_{jet}^3 \times 10^3}$
XIII					
$0.45 \leqslant x/D \leqslant 0.6$					
$\Delta\phi = 0°$	-3.73	0.07	0.23	-0.02	0.16
$\Delta\phi = 90°$	-5.83	0.57	0.20	-0.02	0.15
$\int E_{90°} - \int E_{0°}$	-2.10	0.50	-0.03	0.00	-0.01
III					
$0.54 \leqslant x/D \leqslant 0.725$					
$\Delta\phi = 0°$	-7.00	1.41	0.19	-0.02	0.24
$\Delta\phi = 90°$	-1.70	0.23	0.22	-0.00	0.27
$\int E_{0°} - \int E_{90°}$	-5.30	1.18	-0.03	-0.02	-0.03
III					
$0.775 \leqslant x/D \leqslant 0.9$					
$\Delta\phi = 0°$	-3.30	0.24	-0.19	-0.00	0.23
$\Delta\phi = 90°$	-5.62	1.11	-0.26	-0.00	0.45
$\int E_{90°} - \int E_{0°}$	-2.32	0.87	-0.07	-0.00	0.22
VI					
$0.5 \leqslant x/D \leqslant 0.66$					
$\Delta\phi = 0°$	-5.99	0.72	0.37	-0.01	0.07
$\Delta\phi = 90°$	-5.55	0.57	0.37	-0.01	0.06
$\int E_{0°} - \int E_{90°}$	0.44	0.15	0.00	0.00	0.01

TABLE 3. Comparison of the streamwise integrals of kinetic energy for three major cases.

The estimated energy exchange from the fundamental to the subharmonic in the range $0.54 \leqslant x/D \leqslant 0.725$ accounts for only a possible 3% contribution to the amplification of the subharmonic.

Beginning at a streamwise position of $x/D = 0.825$, the subharmonic wave gains energy up to $x/D = 1.0$. The subharmonic wave in the initially amplified case with $\Delta\phi = 0°$ gains little in this region when compared with the subharmonic gain for the suppressed case of $\Delta\phi = 90°$. Even in this region the possible contribution of the fundamental to the subharmonic amounts to only 9% of the subharmonic growth. The loss in the fundamental may be balanced in part by the gain in random turbulence energy.

For higher amplitude of forcing (case *VI*) no significant differences of the integrated kinetic energy were observed for $\Delta\phi = 0°$ and $\Delta\phi = 90°$. The energy gained or lost by the streamwise turbulence component and by the same component of the coherent waves is never fully balanced by the energy lost by the mean motion; the latter is always larger. The above balance neither takes lateral velocity fluctuations nor the dissipative terms into account. It is, therefore, only a rough estimate which confirms that most of the energy gained by the resonant subharmonic is supplied by the mean flow.

6.3. *The interaction between the mean flow and the coherent motion*

The kinetic energy equations describing a turbulent flow with coherent motion can be obtained by applying a triple decomposition (Hussain & Reynolds 1970) of the

Navier–Stokes and continuity equations and using successively phase- and time-averaging. The resulting equations can be simplified by making the boundary-layer-type approximations (Hinze 1975) to the mean quantities. The diffusion terms vanish upon integration across the flow and the energy equation for the mean motion becomes

$$\frac{1}{2}\frac{\mathrm{d}}{\mathrm{d}x}\int_{r=0}^{r_{0.1}}\overline{U}^3 r\,\mathrm{d}r = -\int_{r=0}^{r_{0.1}} -\overline{\tilde{u}\tilde{v}}\frac{\partial\overline{U}}{\partial r}r\,\mathrm{d}r - \int_{r=0}^{r_{0.1}} -\overline{u'v'}\frac{\partial\overline{U}}{\partial r}r\,\mathrm{d}r. \tag{6.4}$$

The direct viscous dissipation of the mean kinetic energy to thermal energy is very small owing to the small strain rates of the mean flow and is neglected. Equation (6.4) suggests that the mean flow loses kinetic energy to the coherent and to the turbulent motion by the work of the Reynolds stresses against the mean shear.

The integral kinetic energy equation for the random turbulence representing the change in the energy of turbulence with x is

$$\begin{aligned}\frac{1}{2}\frac{\mathrm{d}}{\mathrm{d}x}\int_{r=0}^{r_{0.1}}\overline{U}(\overline{u'^2}+\overline{v'^2}+\overline{w'^2})r\,\mathrm{d}r &= \int_{r=0}^{r_{0.1}} -\overline{u'v'}\frac{\partial\overline{U}}{\partial r}r\,\mathrm{d}r \\ &+ \int_{r=0}^{r_{0.1}}\overline{\frac{\partial\tilde{u}_{i,sub}}{\partial x_j}\underbrace{(-\langle u_i'u_j'\rangle_{sub}+\overline{u_i'u_j'})}_{r_{ij,sub}}}r\,\mathrm{d}r \\ &+ \int_{r=0}^{r_{0.1}}\overline{\frac{\partial\tilde{u}_{i,fun}}{\partial x_j}\underbrace{(-\langle u_i'u_j'\rangle_{fun}+\overline{u_i'u_j'})}_{r_{ij,fun}}}r\,\mathrm{d}r - \int_{r=0}^{r_{0.1}}\overline{\Phi'}r\,\mathrm{d}r.\end{aligned} \tag{6.5}$$

The first term on the right-hand side of equation (6.5), $\int_{r=0}^{r_{0.1}} -\overline{u'v'}(\partial\overline{U}/\partial r)r\,\mathrm{d}r$, appears as a source term representing the production of turbulent energy by the mean flow while it appears with an opposite sign (i.e. as a loss) in the mean energy equation. The second and the third terms are the energy contribution of turbulence to the coherent motion containing mostly the subharmonic and the fundamental waves. The last term Φ' represents the viscous dissipation of random turbulence.

Since only single-wire probes could be calibrated in the facility the radial components were calculated from the decomposed, densely acquired streamwise data using continuity condition (2.3). In order to obtain well-behaved derivatives from the mean velocities the data were interpolated by using the *Akima*-interpolation (Akima 1970) and the resulting derivatives were smoothed in Fourier space. The total Reynolds stress was then calculated from the mean-momentum equation. The coherent data, having only little scatter, provided reasonably smooth derivatives so that only slight additional smoothing was necessary. Having both $\tilde{u}$ and $\tilde{v}$ data over the complete forcing cycle enabled us to calculate the coherent Reynolds stresses by multiplying each value of the phase coherent $\tilde{u}$- and $\tilde{v}$-records and time-averaging of the products.

Fourier decomposition of the phase-coherent data gives the complex eigenmode shape $\hat{u}$ and $\hat{v}$. The wave Reynolds stress is then

$$\overline{\tilde{u}\tilde{v}}|_f = \tfrac{1}{2}\mathrm{Re}(\hat{u}\hat{v}^*) = \tfrac{1}{2}\mathrm{Re}(\hat{u}^*\hat{v}), \tag{6.6}$$

where '$*$' denotes a complex conjugate and Re means 'real part of'.

The production terms of the turbulent energy, the total coherent energy (consisting here of *all* the coherent components in the flow) and the streamwise rate of the change of the energy of the mean motion are displayed in figures 22 to 24. They indicate that the turbulence production by the mean flow is strongly affected by the *amplified*

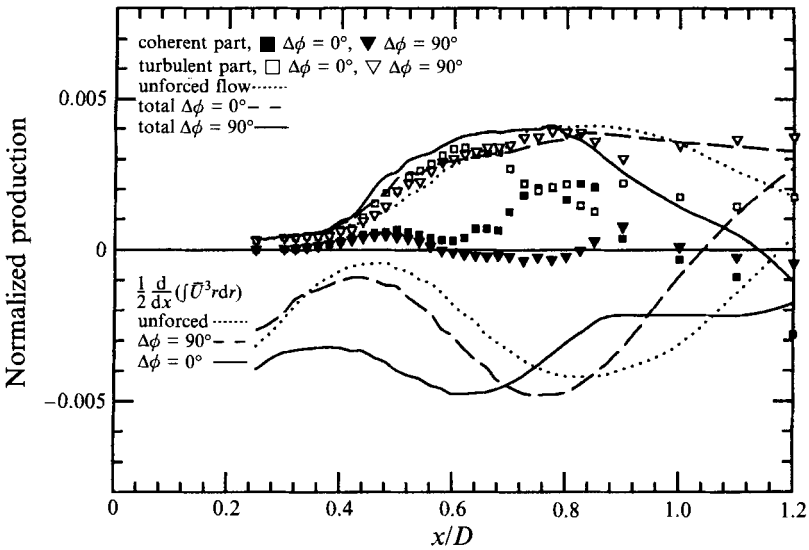

FIGURE 22. Variation of the production terms with x/D, f_{sub} = 184Hz, f_{fun} = 368Hz (case *III*).

subharmonic wave. Positive production represents a gain of the flow component while negative production represents its loss.

For case *III* (shown in figure 22) the coherent productions of the suppressed subharmonic and amplified subharmonic are equal up to $x/D \approx 0.44$. The subsequent increase in the coherent production is attributed to the fast growing fundamental which draws energy from the mean flow on account of the turbulence provided that $x/D \leqslant 0.5$ (e.g. see $x/D = 0.44$). The production terms are linked to the growth rate of the jet. As both coherent and turbulent production determine this growth and their sum is higher than in the unforced case, the momentum thickness increases more rapidly than in the unforced case (figure 19). From $x/D > 0.44$ the coherent production in the case of the amplified subharmonic is larger than the coherent production of the suppressed subharmonic, because of the amplification of the subharmonic wave in the former case.

The coherent production in the case of the suppressed subharmonic becomes negative at $x/D \approx 0.6$ which corresponds approximately to the position at which the fundamental is neutrally stable according to linear theory. However, some growth of the fundamental is maintained up to $x/D = 0.75$ as is obvious from the evolution of the kinetic energy integrals (figure 21). Beyond $x/D \approx 0.6$ the subharmonic generated at $\Delta\phi = 0°$ is growing fast by diverting energy normally available for the production of random turbulence itself. As a consequence the mean energy and the turbulence production decrease with x. The total coherent production increases and becomes equivalent to the turbulent production at $x/D \approx 0.75$. From $x/D > 0.88$ the production of the highly amplified subharmonic ceases and part of its energy is converted to random motion. Consequently the random Reynolds stress increases and with it the turbulence production, becoming similar in magnitude to the turbulence production of the unforced case at $x/D \approx 1.2$. In the case of the suppressed subharmonic (i.e. $\Delta\phi = 90°$) the coherent production becomes positive around $x/D \approx 0.8$ which results in a slight growth of the subharmonic (figure 21).

A cross-check of the calculated Reynolds stresses can be obtained by comparing the total production of the fluctuating motion by the mean motion with the streamwise

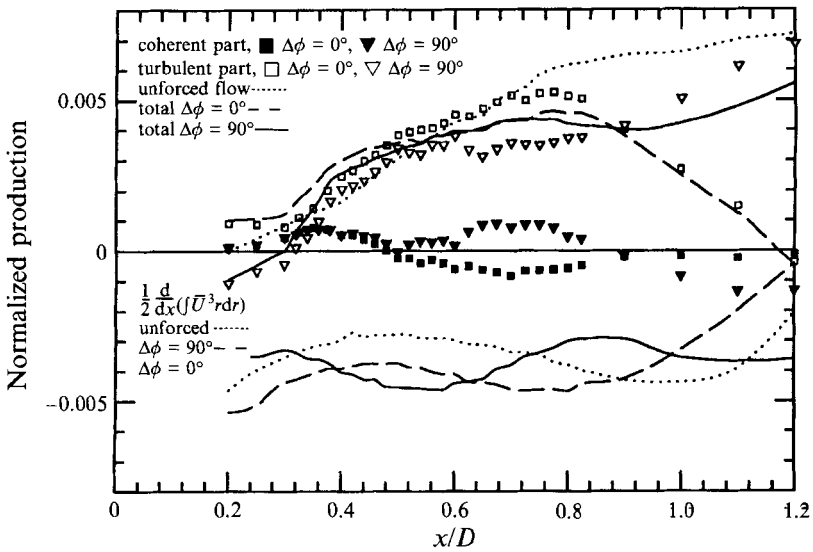

FIGURE 23. Variation of the production terms with x/D, $f_{sub} = 184$Hz, $f_{fun} = 368$Hz, tripwire (case *XIII*).

depletion in the kinetic energy of the mean flow. Following equation (6.4), the term $\frac{1}{2}(\mathrm{d}/\mathrm{d}x)\int_{r=0}^{r_{0.1}} \overline{U}^3 r\,\mathrm{d}r$ must be balanced by the sum of turbulent and coherent production. The derivative of the kinetic energy integral is displayed in figure 22 as a loss term, representing a loss of mean energy to the turbulent and coherent motions by the action of the Reynolds stresses against the mean shear $\partial\overline{U}/\partial r$. The calculated $\int_{r=0}^{r_{0.1}} \overline{uv}(\partial\overline{U}/\partial r)r\,\mathrm{d}r$ and the $\int_{r=0}^{r_{0.1}} \overline{U}^3 r\,\mathrm{d}r$ contain cumulative errors introduced by estimating derivatives from measured quantities. Still, the terms calculated for the unforced flow agree fairly well: the gain of the turbulent field displayed by the production term is balanced by the loss of energy of the mean flow. The agreement was less good when the jet was subjected to the bimodal forcing. The minima of the loss of kinetic energy by the mean motion which are related to the maxima in the gain by the turbulent and the coherent motions do not occur at the same streamwise position but they are shifted upstream by $\lambda/4$.

The production terms for the case of the tripped nozzle flow are displayed in figure 23. There the subharmonic was amplified at $\Delta\phi = 90°$. The coherent production is always smaller when compared to the case without the trip ring while the turbulent production is larger. In the case of the 'suppressed subharmonic' the coherent production is negative from $x/D > 0.5$ suggesting that energy is supplied by the coherent fundamental (being the most prominent term at $x/D \approx 0.5$) back to the mean flow. However, the kinetic energy integral of the fundamental (figure 20) shows a slight increase with x in the region $0.5 \geqslant x/D \geqslant 0.6$. A similar behaviour was also observed for the non-tripped case (*III*) and will be discussed in the following section. The subharmonic level in this case never exceeded the level achieved when the subharmonic alone was forced and thus the total coherent production cannot indicate an actual gain in the coherent components at $x/D > 0.5$.

When examining the high forcing case (case *VI*), we found the evolution of the subharmonic to be insensitive to the initial phase difference and the same was true for the production terms. For the phase differences $\Delta\phi = 0°$ and $\Delta\phi = 90°$ the production terms are identical (figure 24).

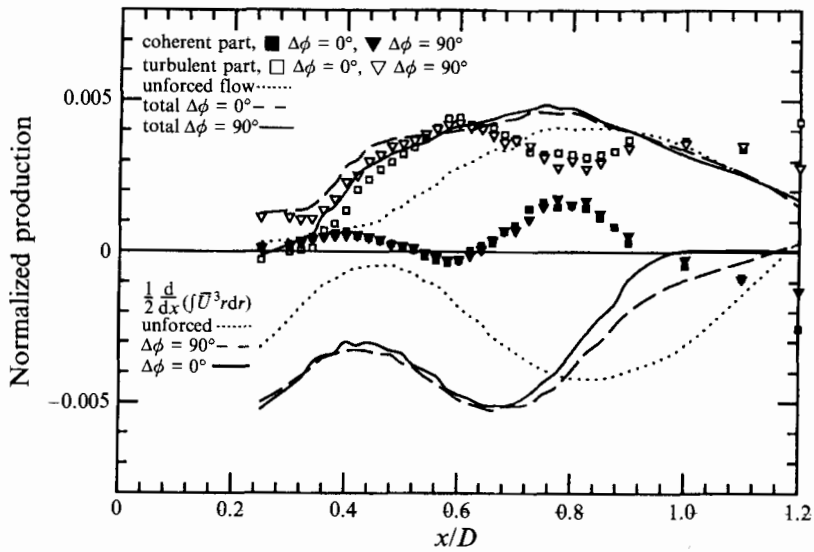

FIGURE 24. Variation of the production terms with x/D, $f_{sub} = 184$Hz, $f_{fun} = 368$Hz, high forcing level (case *VI*).

6.4. *Wave–wave interaction terms*

As it was not possible in the present experiment to measure the interactions among the waves directly, further insight was gained by comparing the coherent wave production by the mean flow. This comparison encompassed only the subharmonic and the fundamental waves. The streamwise changes in the energy of each of the coherent waves considered can be described in the same manner as in equations (6.4) and (6.5).

The integrated energy balance for the fundamental is then

$$\frac{1}{2}\frac{d}{dx}\int_{r=0}^{r_{0.1}} \overline{U}(\overline{\tilde{u}^2}+\overline{\tilde{v}^2}+\overline{\tilde{w}^2})_{fun} r\,dr = \int_{r=0}^{r_{0.1}} -\overline{\tilde{u}\tilde{v}}|_{fun}\frac{\partial \overline{U}}{\partial r}\,r dr$$
$$-\int_{r=0}^{r_{0.1}} \overline{\langle -\tilde{u}_i\tilde{u}_j\rangle_{sub}\frac{\partial \tilde{u}_{i,fun}}{\partial x_j}}\,r\,dr - \int_{r=0}^{r_{0.1}} \frac{\partial \tilde{u}_{i,fun}}{\partial x_j}\underbrace{(-\langle u_i'u_j'\rangle_{fun} + \overline{u_i'u_j'})}_{r_{ij,fun}} r\,dr, \qquad (6.7)$$

and the energy equation for the subharmonic is

$$\frac{1}{2}\frac{d}{dx}\int_{r=0}^{r_{0.1}} \overline{U}(\overline{\tilde{u}^2}+\overline{\tilde{v}^2}+\overline{\tilde{w}^2})_{sub} r\,dr = \int_{r=0}^{r_{0.1}} -\overline{\tilde{u}\tilde{v}}|_{sub}\frac{\partial \overline{U}}{\partial r}\,r\,dr$$
$$+\int_{r=0}^{r_{0.1}} \overline{\langle -\tilde{u}_i\tilde{u}_j\rangle_{sub}\frac{\partial \tilde{u}_{i,fun}}{\partial x_j}}\,r\,dr - \int_{r=0}^{r_{0.1}} \overline{\frac{\partial \tilde{u}_{i,sub}}{\partial x_j}\underbrace{(-\langle u_i'u_j'\rangle_{sub} + \overline{u_i'u_j'})}_{r_{ij,sub}}}\,r\,dr. \qquad (6.8)$$

The fundamental gains energy from the mean flow (first term on the right-hand side of equation (6.7)) and loses energy to the subharmonic (second term) and to random turbulence (third term). The subharmonic gains energy from the mean flow (first term on the right-hand side of (6.8)) and from the fundamental (second term) while losing energy to the turbulent field (third term). The subharmonic loses energy also to other waves, particularly to its own subharmonic (i.e. a frequency which is two octaves lower than the fundamental). Owing to the lack of data for the other velocity

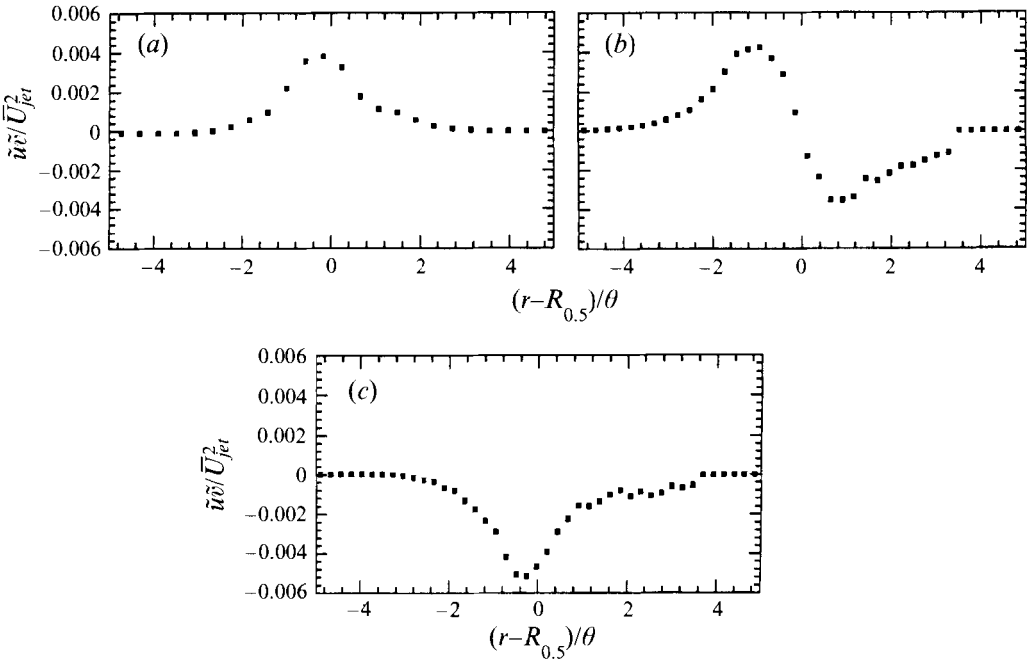

FIGURE 25. The Reynolds stress of the subharmonic in the tripped case (case *XIII*) at three downstream positions corresponding to locations of (*a*) $St_{local} < St_{critical}$, (*b*) $St_{local} \approx St_{critical}$, (*c*) $St_{local} > St_{critical}$. $f_{sub} = 184$Hz, $f_{fun} = 368$Hz.

components (i.e. $\tilde{v}$ and $\tilde{w}$) only an approximate energy balance could be constructed by considering the streamwise component measured, the lateral component $\tilde{v}$ which was calculated from the continuity equation (2.3) and the *uv* correlations.

The Reynolds stresses associated with the coherent wave were calculated from equation (6.6). The distribution of the Reynolds stress of the subharmonic wave is displayed in figure 25 for three typical downstream locations. The linear stability theory predicts that the Reynolds stresses reverse their sign when the local Strouhal number St_θ changes from a value smaller than critical (here critical means one in which the fundamental becomes neutral) (figure 25*a*) to a Strouhal number larger than critical (figure 25*c*). The *S*-shaped distribution, occurring for $St_{local} \approx St_{critical}$ (figure 25*b*), can also be obtained by adding a small nonlinearity to the linear approach (Cohen 1986). The negative Reynolds stresses† may be associated with the inclination of the large eddies, as proposed by Fiedler *et al.* (1980) and by Browand (1980).

The production terms of each wave were calculated from the total coherent Reynolds stress. They are presented in figure 26(*a–c*) and they represent the left-hand term of equations (6.7) and (6.8): $(\frac{1}{2}(\mathrm{d}/\mathrm{d}x)\int_{r=0}^{r_{0.1}} \overline{U}(\overline{\tilde{u}^2}+\overline{\tilde{v}^2})r\,\mathrm{d}r)$. Three different cases are considered, all of them forced at the frequency pair $f_{sub} = 184$ Hz and $f_{fun} = 368$ Hz. Figure 26(*a*) displays the case where the initial amplitude ratio of fundamental and subharmonic was $\gamma = 1.6$ and the flow in the nozzle was not tripped (case *III*). In figure 26(*b*) the flow was tripped for the same initial amplitude ratio of $\gamma = 1.6$

† Zaman & Hussain (1980) related negative Reynolds stresses to regions of vortex pairing. However, Oster & Wygnanski's (1982) results indicate vortex pairing to be inhibited for negative Reynolds stresses.

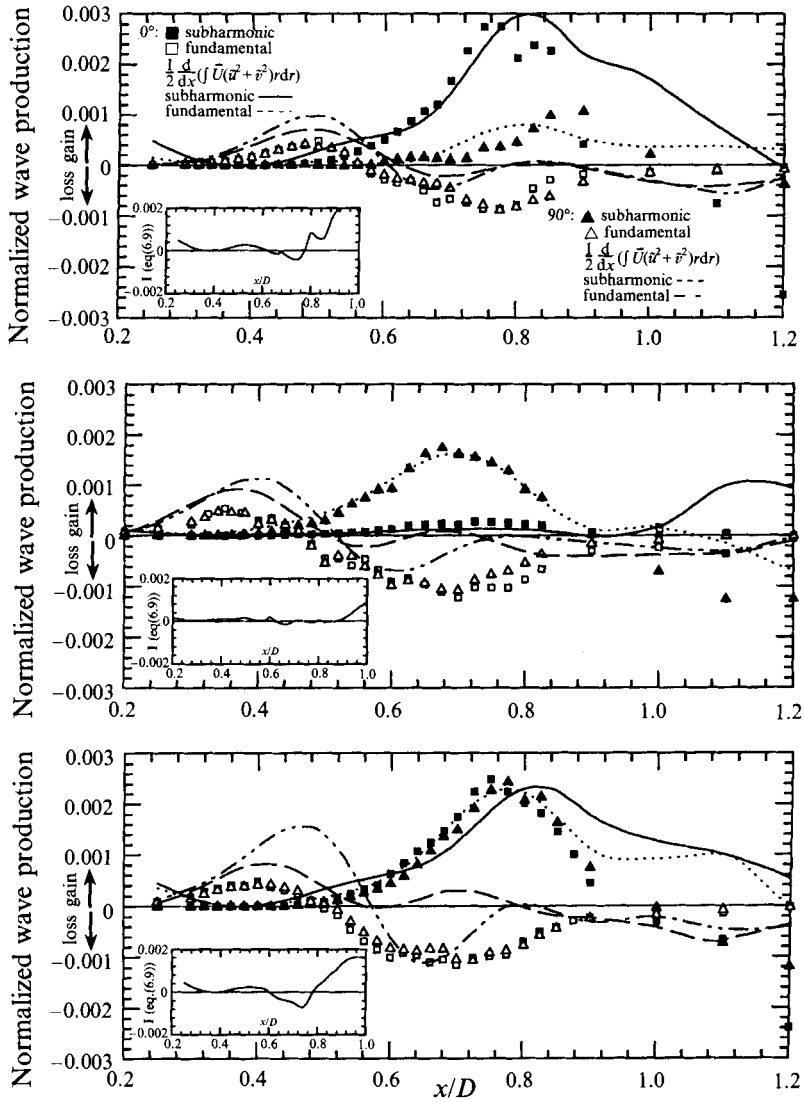

FIGURE 26. Variation of the production terms with x/D, f_{sub} = 184Hz, f_{fun} = 368Hz: (*a*) case *III*, (*b*) tripwire, case *XIII*, (*c*) high forcing level, case *VI*.

and finally the case where the overall forcing level was doubled (case *VI*) is plotted in figure 26(*c*).

The wave production of the fundamental in all three figures is mostly negative at $x/D > 0.5$. This is associated with the negative wave Reynolds stresses of the fundamental wave. The occurrence of negative production terms due to negative total Reynolds stresses as observed by Oster & Wygnanski (1982) was not observed in the present experiment. The total Reynolds stress can only be negative in a zero or negative growth region of the shear layer which did not occur for the investigated, low forcing levels.

In the initial region of the jet (i.e. at $x/D < 0.5$) the production of the fundamental is dominant and therefore the fundamental grows. For the untripped case the fundamental production reaches its maximum at $x/D \approx 0.5$ (figure 26*a*). This

is associated with the maximum growth of the fundamental kinetic energy integral (figure 21). From $x/D \approx 0.58$ the production of the fundamental is negative, indicating energy transfer from the fundamental back to the mean flow. At this streamwise position the fundamental is neutral based on linear stability theory. However, the kinetic energy integral for the fundamental (figure 21) is still slightly growing at this position as is indicated by the positive value of the term $\frac{1}{2}(\mathrm{d}/\mathrm{d}x)\int_{r=0}^{r_{0.1}} \overline{U}(\overline{\tilde{u}^2}+\overline{\tilde{v}^2})r\,\mathrm{d}r$ plotted in figure 26(*a*). For both cases, $\Delta\phi = 0°$ and $\Delta\phi = 90°$, the production of the fundamental by the mean motion is almost identical up to $x/D = 0.8$. The slightly reduced decay of the fundamental in the case of $\Delta\phi = 0°$ is due to the decreasing subharmonic which supplies energy back to the mean flow (figure 20). The production terms of the subharmonic show major differences depending on the initial phase angle. The production of the subharmonic in the suppressed case starts farther downstream at $x/D > 0.72$ and reaches a lower peak value at $x/D = 0.8$. The change in the derivative of the kinetic energy integral is associated with the production of the subharmonic by the mean flow. Both the derivative of the kinetic energy integral and the production of the subharmonic show identical behaviour in the case of the resonant amplified subharmonic. Both terms reach the same maximum value indicating again that most of the energy for the subharmonic is supplied by the mean flow.

An estimate of the energy supplied by the fundamental directly to the subharmonic as described by the term $\int_{r=0}^{r_{0.1}} \overline{\langle -\tilde{u}\tilde{v}\rangle_{sub}(\partial\tilde{u}_{fun}/\partial r)}r\,\mathrm{d}r$ can be obtained by the difference between the derivative of the kinetic energy and the coherent production of subharmonic by the mean flow. This difference

$$\frac{1}{2}\frac{\mathrm{d}}{\mathrm{d}x}\int_{r=0}^{r_{0.1}} \overline{U}(\overline{\tilde{u}^2}+\overline{\tilde{v}^2})_{sub}r\,\mathrm{d}r - \int_{r=0}^{r_{0.1}} -\overline{\tilde{u}\tilde{v}}|_{fun}\frac{\partial\overline{U}}{\partial r}r\mathrm{d}r = \mathrm{I} \tag{6.9}$$

for the resonant amplified subharmonic (i.e. $\Delta\phi = 0°$) is also plotted in figure 26 in the separate window and marked by a solid line. This estimate is smaller than the real fundamental–subharmonic energy transfer, because the subharmonic loses energy to random turbulence. However, this term was shown to be small, particularly in the growth region of the subharmonic (figure 22), which again corroborates the notion that the direct energy transfer from the fundamental to the subharmonic wave is very small indeed.

The case of the tripped nozzle flow (figure 26*b*) shows the same features as described above. The interaction between the instability waves, however, is moved upstream as a consequence of the increase in the rate of spread of the mean flow. The maximum production of the amplified subharmonic occurring at $\Delta\phi = 90°$ is approximately 30% less than for the non-tripped flow (case *III*) while the production of the subharmonic in the suppressed case is negligible throughout.

When the forcing level was doubled (figure 26*c*) no influence of the initial phase difference was found. The stronger forcing immediately led to a phase locking between the two waves irrespective of the initial $\Delta\phi$. The production terms as well as the derivatives of the kinetic energy integrals are identical for both $\Delta\phi$ considered in case *VI*.

6.5. *Random turbulence*

External excitation can suppress or enhance random turbulence, depending on the frequency of forcing. The streamwise development of the maximum in $\overline{u'^2} = \overline{(u-\langle u\rangle)^2}$ is shown in figure 27 for various cases corresponding to $\gamma = 1.6$ in the absence of the trip wire. Note that only the random turbulence component of fluctuating axial

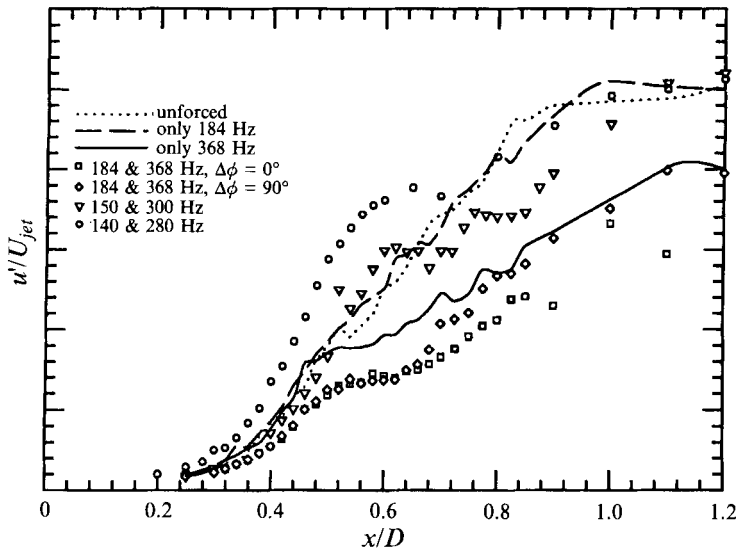

FIGURE 27. Maximum amplitude of random turbulence along x/D for the untripped nozzle

single-frequency forcing corresponding to the 'subharmonic' frequency of $f = 184$ Hz ($St_{D,sub} = 1.2$) relative to the unforced flow (figure 27). Conversely, when the jet was forced at the fundamental frequency of $f = 368$ Hz ($St_{D,fun} = 2.3$) the random turbulence is suppressed from $x/D \approx 0.48$. This is in accordance with the observations of Zaman & Hussain (1981) and the theoretical investigation of Mankbadi (1985) who have shown that turbulence suppression occurs for higher Strouhal numbers $1.2 < St_D < 2.4$, where $St_D = fD/\nu$. Bimodal forcing of the jet at 184 Hz and 368 Hz with an initial amplitude ratio of $\gamma = 1.6$ also shows suppression of random turbulence, which in the case of the resonant amplified subharmonic ($\Delta\phi = 0°$ for case *III*) is most pronounced.

The calculated incoherent production by the mean motion for the forced and the unforced flow is almost identical for both cases around $x/D \approx 0.48$ where the drop in the turbulent fluctuations occurs. As the fundamental continues to grow downstream of this x-position (as may be deduced from the development of the term $\frac{1}{2}(\mathrm{d}/\mathrm{d}x)\int_{r=0}^{r_{0.1}} \overline{U}(\overline{\tilde{u}^2} + \overline{\tilde{v}^2})|_{fun} r\,\mathrm{d}r$), although the coherent production of the fundamental by the mean motion becomes negative and it detracts from the growth of the fundamental, energy may be transferred directly from the turbulent field to the fundamental as described by the term $r_{fun} = -\langle uv\rangle + \overline{u'v'}$. However, as no phase-locked data for the turbulent Reynolds stresses were available, the coherent–turbulent energy transfer by the action of r_{fun} can not be verified. One may conclude, from the available data, that the strong drop in turbulence is mostly associated with the fundamental wave. Single-frequency forcing at the subharmonic frequency and the presence of an amplified subharmonic in the bimodal forcing cases had only a minor effect on the background turbulence.

From $x/D > 0.7$ the fundamental is decaying partly by losing its energy to random turbulence through the coherent↔random interaction. Thus the turbulence intensities can continue to grow while the turbulent production by the mean is decreased (figure 22). The effect of random turbulence suppression as a result of excitation is even more pronounced when the jet is forced at higher amplitudes or when the flow is tripped (figure 28). For the tripped nozzle flow the random↔coherent energy transfer

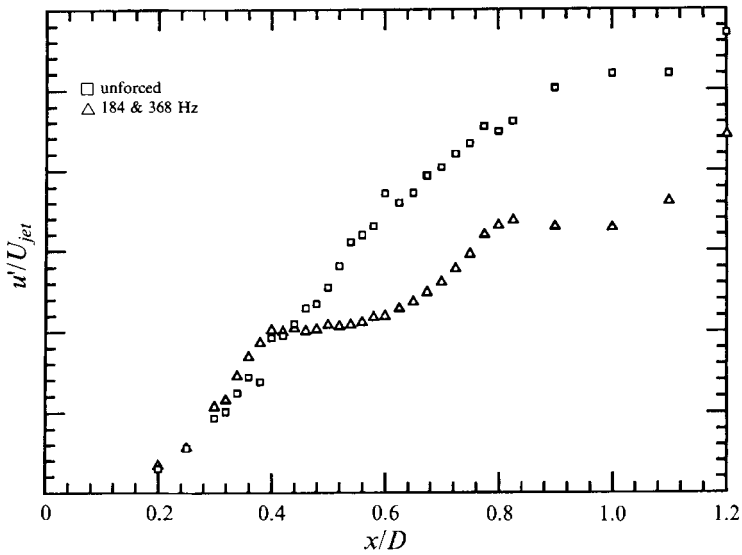

FIGURE 28. Maximum amplitude of random turbulence along x/D for the tripped nozzle

to the subharmonic occurs at $x/D \approx 0.9$ because of the term $r_{sub} = -\langle uv \rangle + \overline{u'v'}$. The turbulence production is positive but the turbulence intensities saturate. The subharmonic wave starts to grow again at this downstream position while the coherent production becomes negative. This suggests that energy is being transferred from the turbulent field to the subharmonic. At $x/D \approx 1.1$ the subharmonic decays and thus the transfer is reversed to the turbulent flow.

Conversely, data taken at lower Strouhal numbers $St_{D,sub} = 0.89$ and $St_{D,fun} = 1.8$ (case XIV) show local enhancement of the jet turbulence when compared to the unexcited case (figure 27) owing to the coherent–random turbulence interaction terms r_{sub} and r_{fun} (equation (6.5)).

Data taken at Strouhal numbers $St_{D,sub} = 0.95$ and $St_{D,fun} = 1.9$ (case XV) with a resonant subharmonic can show either increased random turbulence or suppressed random turbulence (figure 27). The fundamental component leads to an enhancement of turbulence up to $x/D \approx 0.6$ while it loses energy through the term r_{fun}. The subharmonic is strongly growing from $x/D > 0.6$ (see figure 14) and drains energy from the mean flow. As a result there is less mean energy available for turbulence production. The subharmonic starts to decay from $x/D \approx 0.85$ and energy is transferred to random turbulence. The above comments about the coherent and random fluctuations are based on the definitions presented in equation (2.1). Phase-locked data tend to reduce the intensity of the coherent motion because they do not account for phase jitter. Thus although the present discussion is statistically valid it may be overemphasizing the significance of the random motion.

7. Concluding remarks

Kelly's (1967) idea of subharmonic resonance was applied and tested in the mixing layer of an axisymmetric jet. The conditions for the resonance were verified experimentally and found to be valid (i.e. the fundamental and the subharmonic are non-dispersive while the linear amplification rate of the fundamental was vanishingly small). The present investigation also demonstrated the importance of the initial

phase difference $\Delta\phi$ between the two externally excited waves on the resonance. It was shown that absolute forcing levels, initial amplitude ratios γ, forcing frequencies, and the characteristic width of the mixing layer (i.e. the initial momentum thickness which can be altered by using a trip ring or a different nozzle), affect the amplitude gain of the subharmonic wave.

At certain initial phase differences $\Delta\phi$ a suppression of the resonant growth of the subharmonic could be observed in spite of the change in the local width of the shear layer which was increased by the trip ring. The intensity of the incoherent motion (i.e. background turbulence) has no significant effect on the growth of the coherent components of the motion. An increase in the forcing level reduces the influence of the initial phase difference on the amplification of the subharmonic. Contour plots of the phase difference $(2\phi_{sub} - \phi_{fun})$, used to describe the degree of non-dispersiveness between the subharmonic and the fundamental, indicate that at higher forcing levels the location at which the two waves became non-dispersive was moved upstream and became independent of the initial phase angle.

Estimates of the energy transfer between the mean motion and the instability waves show that most of the energy gained by the subharmonic is supplied by the mean flow directly. The sensitivity of the amplification of the subharmonic to the location at which the two forced waves become non-dispersive is surprising in view of the fact that the energy for the growth of this wave comes from the mean motion. It is also noted that the subharmonic wave generated by the resonance alters the streamwise development of the mean flow by decreasing its overall kinetic energy and increasing the momentum thickness. Theoretical models neglecting this interaction (Kelly 1967; Cohen & Wygnanski 1987; Monkewitz 1988) by assuming the flow to be parallel miss an important feature of the subharmonic resonance mechanism. Hence one of the purposes of the present experiment was to stimulate more accurate theoretical predictions. The nonlinear energy integral technique used by Mankbadi & Liu (1981) describes at best some changes in the mean flow and the influence of the subharmonic on the fundamental. Their model predicts that an increase in the forcing level reduces the influence of the initial phase difference on the growth of the subharmonic. However, Mankbadi (1991) relates this phenomenon to a decrease in the wave–wave interaction and an increase in the importance of the mean-flow–wave energy transfer. This was not observed in the present experiment. The maximum normalized energy drained from the mean flow at the higher forcing level was 0.0026 at $x/D = 0.75$ while at a lower forcing level (showing an influence of the initial phase difference) the normalized energy drained was actually 0.0028 and occurred at $x/D = 0.775$ (see figure 26). This indicates that no increase of the mean-flow↔wave interaction is necessary at higher forcing levels.

An important difference between the present work and other similar experiments is in the very low forcing level used here. The amplitude of the phase-locked fundamental never exceeded 0.02% on the centreline at $x/D = 0.25$, while it was around 1.4% in the experiment of Bradly & Ng (1989) and 2% in the experiment of Arbey & Ffwocs Williams (1984). Since there is more than one way in which a resonance may be realized, the correct mechanism involved is not easily uncovered. Third-order effects may be of importance and perhaps may even dominate the flow, if one of the waves exceeds a certain threshold level.

Artificial excitation of the flow by two frequencies separated by one octave may have many practical applications because it offers a tool to control the turbulence structure and the spreading rate of a mixing layer beyond the possibilities associated with single-frequency excitation. Thus the flow can be controlled by changing the

with single-frequency excitation. Thus the flow can be controlled by changing the excitation frequency, the overall forcing level, the relative phase angle and forcing ratio between the two wave trains. The amplification rate of the subharmonic and the maximum amplitude of the subharmonic attained (which affects the spread of the mixing layer) is controlled by the initial phase angle between the two input waves.

REFERENCES

AKIMA, H. 1970 A new method of interpolation and smooth curve fitting based on local procedures. *J. Assoc. Comput. Machinery* **17**, 589–602.

ARBEY, H. & FFOWCS WILLIAMS, J. E. 1984 Active cancellation of pure tones in an excited jet. *J. Fluid Mech.* **149**, 445–454.

BATCHELOR, G. K. & GILL, A. 1962 Analysis of the stability of axisymmetric jets. *J. Fluid Mech.* **14**, 529.

BRADLY, T. A. & NG, T. T. 1989 Phase-locking in a jet forced with two frequencies. *Exp. Fluids* **7**, 38–48.

BROWAND, F. K. 1980 A physical description of the turbulent mixing layer. *Bull. Am. Phys. Soc.* **25**, 1102.

COHEN, J. 1986 Instabilities in turbulent free shear flows. PhD thesis, University of Arizona, USA.

COHEN, J. & WYGNANSKI, I. 1987*a* The evolution of instabilities in the axisymmetric jet. Part 1. The linear growth of disturbances near the nozzle. *J. Fluid Mech.* **176**, 191–219.

COHEN, J. & WYGNANSKI, I. 1987*b* The evolution of instabilities in the axisymmetric jet. Part 2. The flow resulting from the interaction between two waves. *J. Fluid Mech.* **176**, 221–235.

CROW, S. C. & CHAMPAGNE, F. H. 1971 Orderly structure in jet turbulence. *J. Fluid Mech.* **48**, 567.

FIEDLER, H. E., DZIOMBA, B., MENSING, P. & RÖSGEN, T. 1980 Initiation, evolution and global consequences of coherent structures in turbulent shear flows. In *The Role of Coherent Structures in Modelling Turbulence and Mixing* (ed. J. Jimenez). Lecture Notes in Physics, pp. 219–251. Springer.

FIEDLER, H. E. & MENSING, P. 1985 The plane turbulent shear layer with periodic excitation. *J. Fluid Mech.* **150**, 281–309.

FREYMUTH, P. 1966 On transition in a separated laminar boundary layer. *J. Fluid Mech.* **25**, 683.

FUCHS, H. V. 1972 Space correlations of the fluctuating pressure in subsonic turbulent jets. *J. Sound Vib.* **23**, 77.

GASTER, M., KIT, E. & WYGNANSKI, I. 1985 Large-scale structures in a forced turbulent mixing layer. *J. Fluid Mech.* **150**, 23–39.

HAJJ, M. R., MIKSAD, R. W. & POWERS, E. J. 1993 Fundamental–subharmonic interaction: effect of phase relation. *J. Fluid Mech.* **256**, 403–426.

HINZE, J. O. 1975 *Turbulence*, 2nd edn. McGraw-Hill.

HUSSAIN, A. K. M. F. & REYNOLDS, W. C. 1970 The mechanics of an organized wave in turbulent shear flow. *J. Fluid Mech.* **41**, 241–258.

KELLY, R. E. 1967 On the resonant interaction of neutral disturbances in inviscid shear flows. *J. Fluid Mech.* **31**, 789.

LONG, T. A. & PETERSEN, R. A. 1992 Controlled interactions in a forced axisymmetric jet. Part 1. distortion of the mean flow. *J. Fluid Mech.* **235**, 37–55.

MANKBADI, R. R. 1985 On the interaction between fundamental and subharmonic instability waves in a turbulent round jet. *J. Fluid Mech.* **160**, 385–419.

MANKBADI, R. R. 1991 Multifrequency excited jets. *Phys Fluids* **3**, 595–605.

MANKBADI, R. & LIU, J. T. C. 1981 A study of the interactions between large-scale coherent structures and fine-grained turbulence in a round jet. *Phil. Trans. R. Soc. Lond.* A **298**, 541–602.

MATTINGLY, G. E. & CHANG, C. C. 1974 Unstable waves on an axisymmetric jet column. *J. Fluid Mech.* **65**, 541.

MICHALKE, A. 1965 On spatially growing disturbances in an inviscid shear layer. *J. Fluid Mech.* **23**, 521.

MICHALKE, A. 1971 Instabilität eines kompressiblen runden Freistrahls unter Berücksichtigung des Einflusses der Strahlgrenzschichtdicke. *Z. Flugwiss.* **19**, 319–328.

MICHALKE, A. 1972 An expansion scheme for the noise from circular jets. *Z. Flugwiss.* **20**, 229–237.

MICHALKE, A. 1977 On the effect of spatial source coherence on the radiation of jet noise. *J. Sound Vib.* **55**, 377–394.

MICHALKE, A. 1984 Survey on jet instability theory. *Prog. Aerospace Sci.* **21**, 159–199.

MICHALKE, A. 1992 On the effect of external flow and shear-layer thickness on the expansion cells of under-expanded supersonic circular jets. *Eur. J. Mech.* B/*Fluids* **11**, 363–382.

MIKSAD, R. W. 1972 Experiments on the nonlinear stages of free shear layer transition. *J. Fluid Mech.* **56**, 695–719.

MIKSAD, R. W. 1973 Experiments on nonlinear interactions in the transition of a free shear layer. *J. Fluid Mech.* **59**, 1–21.

MONKEWITZ, P. A. 1982 On the effect of the phase difference between fundamental and subharmonic instability in a mixing layer. *Internal rep., Univ. of California, Los Angeles.*

MONKEWITZ, P. A. 1988 Subharmonic resonance, pairing and shredding in the mixing layer. *J. Fluid Mech.* **188**, 223–252.

ORSZAG, S. A. & PATERA, A. T. 1983 Secondary instability of wall-bounded shear flows. *J. Fluid Mech.* **128**, 347–385.

OSTER, D. & WYGNANSKI, I. 1982 The forced mixing layer between parallel streams. *J. Fluid Mech.* **123**, 91–130.

PASCHEREIT, C. O., OSTER, D., LONG, T. A., FIEDLER, H. E. & WYGNANSKI, I. 1992 Flow visualization of interactions among large coherent structures in an axisymmetric jet. *Exps. Fluids* **12**, 189–199.

PATNAIK, P. C., SHERMAN, F. S. & CORCOS, G. M. 1976 A numerical simulation of Kelvin–Helmholtz waves of finite amplitude. *J. Fluid Mech.* **73**, 215–240.

PETERSEN, R. A. 1978 Influence of wave dispersion on vortex pairing in a jet. *J. Fluid Mech.* **89**, 469–495.

PLASCHKO, P. 1979 Helical instabilities of slowly divergent jets. *J. Fluid Mech.* **92**, 209–215.

RAMAN, G. & RICE, E. J. 1989 Subharmonic and fundamental high-amplitude forcing of an axisymmetric jet. *AIAA Paper* 89-0993.

ROBERTS, F. A. 1984 Effect of a periodic disturbance on structure and mixing in turbulent shear layers and wakes. PhD thesis, California Institute of Technology, USA.

RONNEBERGER, D. & ACKERMANN, U. 1979 Experiments on sound radiation due to nonlinear interactions of instability waves in a turbulent jet. *J. Sound Vib.* **62**, 121–129.

STRANGE, P. J. R. 1981 Spinning modes in orderly jet structure and jet noise. PhD thesis, University of Leeds, UK.

WEISBROT, I. & WYGNANSKI, I. 1988 On coherent structures in a highly excited mixing layer. *J. Fluid Mech.* **195**, 137–159.

ZAMAN, K. B. M. Q. & HUSSAIN, A. K. M. F. 1980 Vortex pairing in a circular jet under controlled excitation. Part 1. General jet response. *J. Fluid Mech.* **101**, 449–491.

ZAMAN, K. B. M. Q. & HUSSAIN, A. K. M. F. 1981 Turbulence suppression in free shear flows by controlled excitation. *J. Fluid Mech.* **103**, 133–159.